Neutrino induced background studies for the SHiP experiment

Masterthesis

Faculty of Science
of the

University Zurich

Nathalie Chételat

University of Zurich[UZH]

Prof. Dr. Nicola Serra
Dr. Barbara Storaci

Zurich
December 2015

Abstract

The Search for HIdden Particles (SHiP) experiment, proposed to be located at Super Proton Synchrotron (SPS) at European Organization for Nuclear Research (CERN), is a new fixed target experiment designed to search for light, long living particles non-present in the Standard Model (SM). One of the main goal of the SHiP experiment is to look for Heavy Neutral Leptons (HNL) particles in the GeV region, as for instance those predicted by the ν Minimal Standard Model (νMSM) [1]. The experiment consists of a large, elliptical decay volume (50 m length and a minor axis of 5 m and a 10 m major axis) and a spectrometer. Inside the decay volume the pressure is set to 10^{-6} bar to suppress interactions. The signal signature of the signal are two charged particles originating from an isolated vertex, located in the decay volume with momenta pointing back to the target. This thesis studies one of the main backgrounds consisting of neutrinos interacting in the vicinity of the decay volume. In addition, the possibility to operate at atmospheric pressure is studied. The pressure inside the decay volume sets demanding and costly requirements to the Hidden Sector (HS) spectrometer. We found that this background can be rejected by placing kinematic, geometrical and veto requirements. This would allow to relax the vacuum requirements, allowing to significantly reduce the cost of the experiment.

Contents

1 Introduction and SHiP overview

Since the discovery of the Higgs Boson in 2012 [2, 3] all particles predicted by the SM have been experimentally observed. The SM provides a consistent description of Nature's elementary particles with three of the four [1] fundamental interactions: the electromagnetic, strong and weak interaction [4]. Nevertheless there are some open questions, which the SM fails to explain. In particular the SM does not explain:

- How the large asymmetry between baryon and anti-baryon in the present Universe arises from a symmetric initial state (BAU)
- What is Dark Matter (DM)
- How neutrinos acquire mass and why are neutrino masses so small

Those questions can be answered by extending the SM, adding undiscovered particles. These extensions of the SM are often referred to as New Physics (NP) or physics Beyond the Standard model (BSM). The search for NP is divided in two frontiers. The first looks for new particles with large masses (energy frontier). This approach is mostly exploited at general purpose experiments at Large Hadron Collider (LHC) and other Future Hadron Colliders (FHC). The others look for new particles in the same mass range as SM particles but with much weaker coupling. To detect these 'Hidden Sector' particles, experiments reaching new limits in intensity are needed, exploring the 'intensity frontier' regions. This concept is schematically illustrated in Figure 1.1.

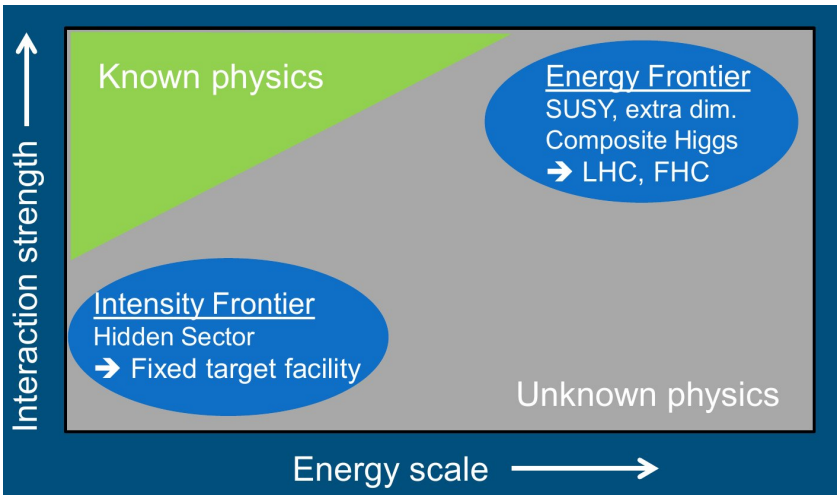

Figure 1.1: Schematic representation of the search for NP at the energy and intensity frontier. Physics BSM could be at low couplings or at high energies. [5]

Since the Higgs boson has a mass that makes the SM a self consistent, weakly coupled theory up to very high energy scales, close to the Planck scales, we can not infer what

[1] Gravity couples very weakly compared to the other fundamental interactions, which makes it negligible (the ratio $^{\text{gravity}}/_{\text{electromagnetism}} = 10^{-39}$). In addition there is no existing, coherent theory of quantum gravity.

the energy scale of NP is. An interesting approach to extend the SM is the 'Minimality principle', which adds the smallest possible set of new fields to the SM particles[2]. The νMSM [1, 7] (discussed in section 2.1) is one of these theories. It adds three, right-handed neutrinos, also called HNLs or sterile neutrinos, to the SM. The HNLs can explain the Baryon-Antibaryon asymmetry (BAU), neutrino masses and DM.

SHiP is a newly proposed fixed target experiment to search for particles of the secluded sector and will be located at SPS of CERN. The SHiP Physics Proposal [5] describes the full physics case for the SHiP experiment. One of the main goal of the SHiP experiment is to search for sterile neutrinos in the GeV region, like those predicted by the νMSM. Another goal is to perform precise measurements of ν_τ physics, which is achieved equipping the facility with an OPERA-like ν_τ-detector. The high intensity beam from the SPS allows to probe many different models with long-lived exotic particles with masses below $\mathcal{O}(10)$ GeV/c^2. With the possibility of an upgrade, also direct dark matter searches and Lepton Flavor Violation decays of τ could be studied later at the same facility.

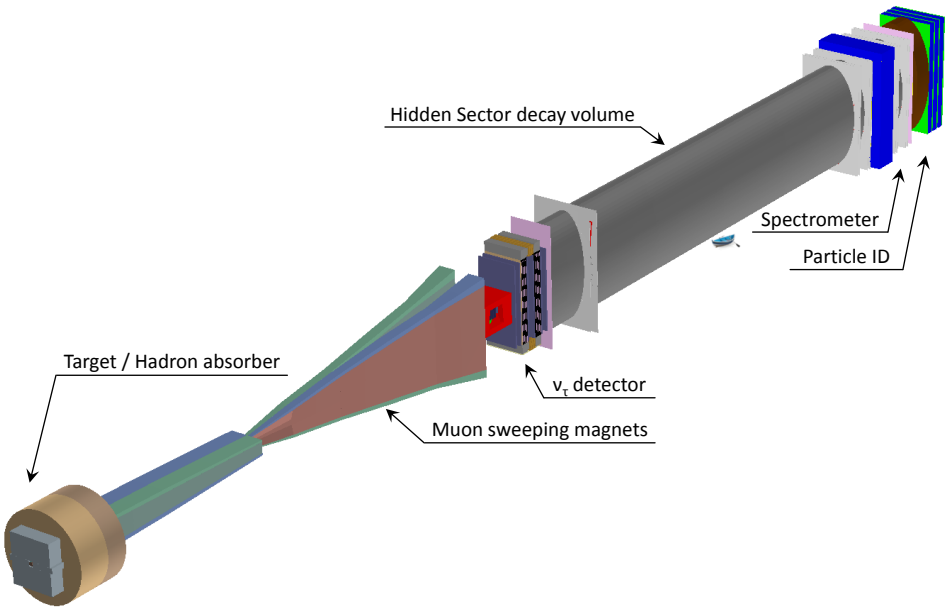

Figure 1.2: Overview of the SHiP experiment [8]

In Figure 1.2 an overview of the SHiP experiment is shown. It consists of a proton target (discussed in section 3.1) of about 1.3 m length in z-direction, which is the direction of the beam axis. The other two axis are looking horizontally (x-direction)

[2] At time of writing ATLAS and CMS presented the result of RUN I. There is a hint of a possible new resonant in the di-photon spectrum at 750 GeV. Since the statistical significance is too low to claim the existence of a new particle this possible new fundamental particle is not considered here. [6]

and vertically (y-direction). To reduce the muon flux in the detector, an active muon shield (discussed in section 3.2) is placed after the target. The muon shield is followed by a ν_τ-detector (discussed in section 3.3) consisting of a ν_τ-target in a magnet and tracking stations also equipped with a magnet (discussed in section 3.3). Following the ν_τ-detector is the HS decay vessel and the HS spectrometer (discussed in section 3.4.2) with particle identification detectors placed at the end. The decay volume has an elliptical shape with the major axis placed in y-direction and having a length of 10 m, while the minor axis has a length of 5 m and is oriented along the x-direction. These are the dimension of the inner walls, for the outer walls additional 30 cm have to be added around the whole vessel. The systems for particle identification, momentum and energy measurement are a tracking station, an electromagnetic calorimeter (ECAL), a hadronic calorimeter (HCAL) and a muon spectrometer (all discussed in section 3.5). This thesis will focus on the νMSM theory and the 'para-photons' theory [9]. However, there are several other models predicting the existence of long lived, very weakly interacting particles [5] and sterile neutrinos in the GeV region.
The goal of this thesis is to study the main background of the SHiP experiment, which is the neutrino induced background. In particular this thesis studies the vacuum requirements of the decay volume, which put severe technological constraints on the experiment.

2 Theory

The SHiP experiment is optimized to discover particles from the secluded sector. The "golden channels" of the SHiP experiment are sterile neutrinos in the GeV region and Dark Photon (DP) with masses below 10 GeV, which are discussed below.

2.1 νMSM

The νMSM [1] extends the SM with three right-handed neutrinos, also called HNLs or sterile neutrinos. The elementary particles of the νMSM are shown in Figure 2.1.

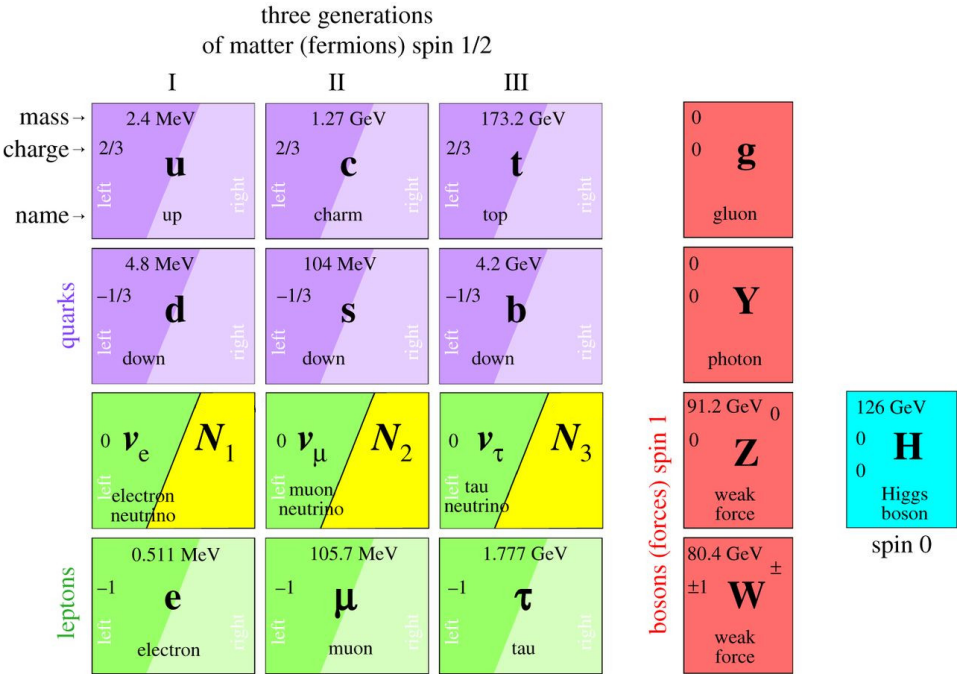

Figure 2.1: The particle content of the νMSM is shown. Three right-handed neutrinos (N_1, N_2, N_3) are added to the SM particles. [5]

The HNLs are singlets under all SM gauge groups. Three scenarios in which HNLs can explain the Baryon-Asymetry at the beginning of the Universe (BAU), neutrino oscillations and the smallness of the SM neutrino masses are discussed below. The first two scenarios also aim to explain the DM with one of the three sterile neutrinos, thus restricting the allowed parameter space, while the last one does not require to explain the DM with the HNLs. The scenarios are:

1. The lightest, right-handed neutrino (N_1) is the DM candidate, while the heavier ones ($N_{2,3}$) allow to explain the observed BAU and active neutrino oscillations. In this scenario the neutrinos are produced thermally and N_1 by a resonant decay of $N_{2,3}$.

2. Also in this scenario N_1 is a DM candidate and $N_{2,3}$ are responsible for the

neutrino oscillations and BAU. However, the right abundance of N_1 is produced by some additional mechanism (e.g. inflaton decay).

3. In the last scenario N_1 is not a DM candidate. This would mean, that all HNLs can participate in the seesaw mechanism. The DM will have to be explained by another unknown particle. This relaxes the constraints on the interactions strength and masses of the three sterile neutrinos.

This νMSM scenario is described by the following Lagrangian:

$$\mathcal{L}_{\nu MSM} = \mathcal{L}_{SM} + i\bar{N}_I \partial\!\!\!/ N_I - \left(Y_{\alpha I} \bar{L}_\alpha N_I \tilde{\Phi} + \frac{M_I}{2} \bar{N}_I^C N_I + h.c. \right) \tag{2.1}$$

Here $\mathcal{L}_{SM}$ is the SM Lagrangian, L_α are the SM lepton doublets and Φ the Higgs doublet, M_I is the Majorana mass for the right-handed neutrinos N_I, with $Y_{\alpha I}$ being the Yukawa coupling. The Dirac mass m_D is defined as the product of the Yukawa coupling $Y_{\alpha I}$ and the Higgs vacuum expectation value $\nu = \sqrt{2}\langle\Phi\rangle$. The presence of a Majorana and a Dirac mass generates mixing terms between active and sterile neutrinos. The mass eigenstates can be found by diagonalizing the mass matrix $M_{\nu,N}$.

$$M_{\nu,N} = \left(\begin{array}{c|c} 0 & m_D \\ \hline m_D & M_I \end{array} \right) \tag{2.2}$$

The sub matrices are the Dirac mass matrix m_D and the Majorana mass matrix M_I. If the matrix $M_{\nu,N}$ was diagonal, there would be no neutrino oscillations. When $M_I \gg m_D$ three of the six eigenvalues have a value $\sim M_I$ and the other three eigenvalues are $\sim \frac{m_D^2}{M_I}$. This is known as the seesaw mechanism [10], which can explain the smallness of neutrino masses.

Unfortunately, the seesaw mechanism does not point out to a particular physics case, since there the Yukawa coupling and the Majorana mass are independent parameters and there are many different combination which allows to generate active neutrino masses in the range 0.12 to 0.25 eV, as determined by the experiments [13]. In the SM the Yukawa coupling of charged fermions ranges from ~ 1 (for the top quark) to $\sim 10^{-5}$ (for the electron), resulting in the masses shown in Figure 2.2. Since the SM particles have only Dirac masses and the Yukawa coupling is proportional to it, the Figure 2.2 also shows the distribution of the Yukawa couplings for different fermions. Without the seesaw mechanism, Yukawa couplings of the order of 10^{-10} would be required to explain the masses of < 0.3 eV. This seems to point out to a separate energy scale. The Yukawa coupling of ~ 1 would require Majorana masses of $\mathcal{O}(10^{14}$ GeV) in order to generate the right scale for active neutrino masses, while Majorana masses of the order of 1 GeV would imply Yukawa couplings of the order of 10^{-6} (one magnitude smaller than the coupling of the electron, as shown in Figure 2.3). The interactions

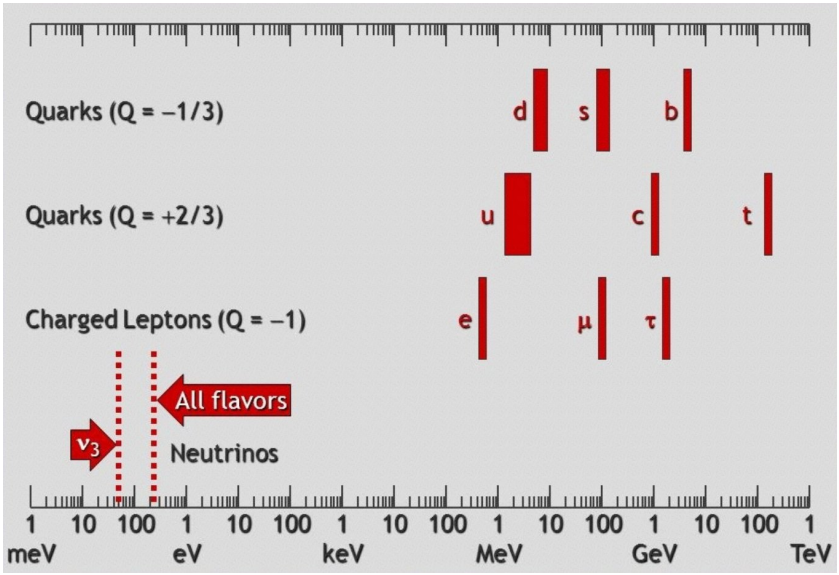

Figure 2.2: Mass of SM fermions (including neutrinos). The upper limit to the neutrino mass range comes from the Planck experiment [11] to the sum of the mass of all neutrino flavor, the lower limit comes from the smallest DM measured in neutrino oscillations. It is worth mentioning that since there are only two DM one the three active neutrinos can be massless. [12]

strengths defines the mixing between the HNLs and the active neutrinos and can be written as in equation 2.3.

$$U_{\alpha I}^2 \equiv \frac{\nu |Y_{\alpha I}|^2}{M_I^2} \ll 1 \tag{2.3}$$

The mass range for the N_I mass goes from 10^{14} GeV to eV. This thesis will focus on the GeV-scale, because this is the range accessible for SHiP. At this scale the HNL only possesses the Yukawa interactions at the unbroken phase in the early universe and thus is able to explain the BAU. HNLs with these masses do not spoil the main fundamental electroweak observables like the Z-boson invisible width $\Gamma_{Z\to inv}$, because the coupling to the active neutrino will get reduced by the mixing angle $U_{\alpha I}^2$ as the coupling to the HNL contributes additionally. Past experiments, mostly looking for two-body decays of charged mesons and HNL decays, already set upper bounds on the interaction strength U^2 (seen in Figure 2.4). The lower bound for U^2 comes from neutrino oscillation experiments and is robust against theoretical assumptions and are also shown in Figure 2.4.

HNLs have been searched for with different experimental methods: direct searches looking for peaks of HNL decays at colliders and fixed target experiment; indirect searches measuring the end of the energy spectrum of electrons in beta decays and searching for neutrinoless double beta decays. For fixed target experiments (like SHiP) the HNLs are mainly produced in heavy meson decays. The main channels for production of HNLs in the GeV range are (semi)-leptonic decays of D_s and B_s mesons:

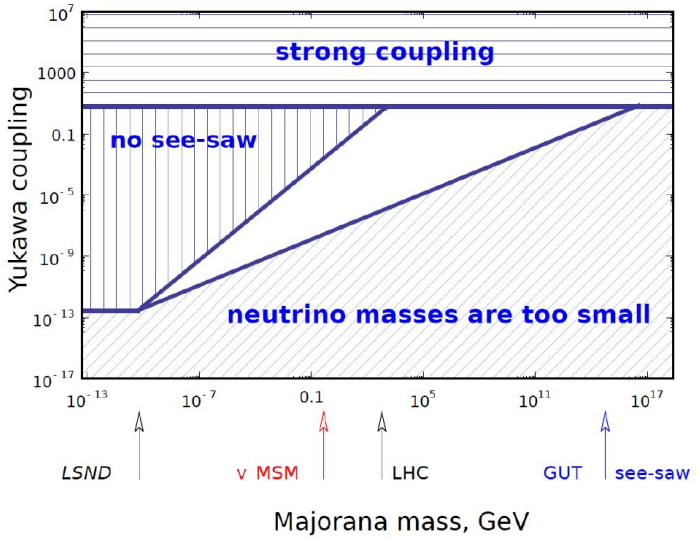

Figure 2.3: Allowed Majorana masses and Yukawa couplings of HNLs in seesaw models. The blue striped regions are forbidden by a theoretical mechanism. [14]

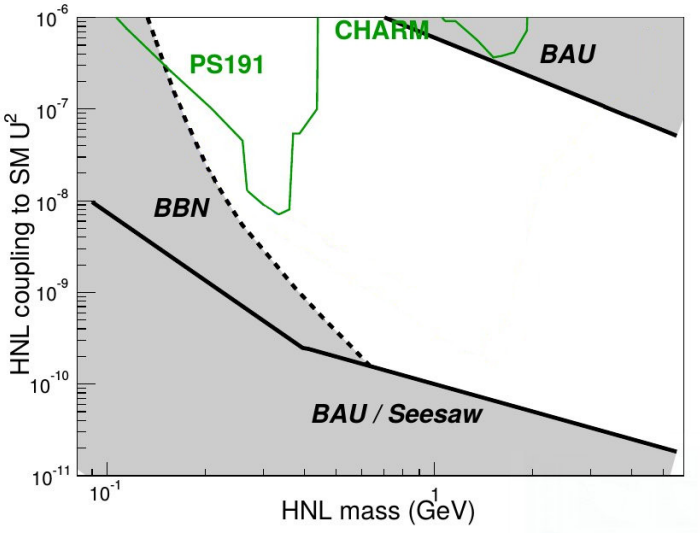

Figure 2.4: Experimental (green) and theoretical (grey) constraints for the HNL coupling to the SM, in the mass range 0 - 10 GeV/c^2 [5]

[14]

$$
\begin{aligned}
&D \to K + l + \text{HNL} \\
&D_s \to l + \text{HNL} \\
&D_s \to \tau + \nu_\tau \text{ followed by } \tau \to l + \nu + \text{HNL}, \pi + \text{HNL} \\
&B \to l + \text{HNL} \\
&B \to D + l + \text{HNL} \\
&B_s \to D_s + l + \text{HNL}
\end{aligned} \tag{2.4}
$$

The decay rate is the same for all weak decays:

$$\Gamma_{N \to weak} \propto |U_{\alpha I}|^2 G_F^2 M_I^5 \tag{2.5}$$

For sterile neutrinos with masses $\mathcal{O}$(1GeV) the allowed decays includes two charged leptons and hadrons in addition to the decay into 3 active neutrinos. In the mass range possible decay channels are:

$$N_I \to e^+ e^- \nu, \mu^+ \mu^- \nu, \mu^\pm e^\mp \nu, \tau^+ \tau^- \nu, \text{ etc.} \tag{2.6}$$

with only lepton final states,

$$N_I \to \pi^\pm e^\mp, \pi^\pm \mu^\mp, K^\pm e^\mp, K^\pm \pi^\mp \nu, \text{ etc,} \tag{2.7}$$

with hadron final states. This allows for two types of direct search experiment looking for HNLs. If the mass of the sterile neutrino is large, it enters in the decay of mesons as a virtual particle and allows decays such as $B^+ \to \mu^+ \mu^+ \pi^-$, that violate lepton number by two units and are the analogous of the neutrinoless double β decays. Here we will concentrate on HNLs with masses of 1 GeV and therefore long lifetimes, which are particularly interesting from a cosmological point of view. In this case the number of signal events is given by:

$$N_S \propto |U_{\alpha I}|^2 \times \frac{l_N}{L_d} \propto |U_{\alpha I}|^4 \tag{2.8}$$

Since the number of sterile neutrinos decaying into the fiducial volume (defined in section 5) is proportional to the forth power of the small mixing parameter $|U_{\alpha I}|$, a high rate of mesons is necessary. This requires a high intensity proton beam as the SPS can provide for SHiP. The experimental signature in direct searches at fixed target experiments (like SHiP) consists of a two track coming from a single vertex, very displaced from the target.

2.2 Dark Photon

If there is an additional $U(1)$ gauge symmetry in the Hidden sector, a Dark Photon (DP) is associated with this symmetry. This particle can mix with SM photon via kinetic mixing and become the mediator between the SM particles and the secluded sector. With the addition of these particles the Lagrangian becomes:

$$\mathcal{L}_{tot} = \mathcal{L}_{SM} + \mathcal{L}_{\chi,A'} - \frac{\epsilon}{2} F_{\mu\nu} F'_{\mu\nu} + \frac{1}{2} m^2_{A'} (A'_\mu)^2 \tag{2.9}$$

Where $\mathcal{L}_{SM}$ is the SM Lagrangian and $\mathcal{L}_{\chi,A'}$ the QED-like hidden sector Lagrangian, ϵ the mixing parameter, $F_{\mu\nu}$ the SM field strength tensor and $F'_{\mu\nu}$ the field strength tensor for the hidden sector particles χ. The last term is the mass term for the DP with $m_{A'}$ being the DP mass and A'_μ the DP field. If the mixing parameter $\epsilon \to 0$ both sectors decouple. Since no DP has been detected yet, the mixing factor ϵ has to be $\ll 1$. For $m_{DP} \to 0$, the states χ can be "millicharged particles" with electric charges $q_\chi = e\epsilon$. The Feynman diagram for a basic interaction between a SM particle and the "millicharged particle" χ is shown in Figure 2.5.

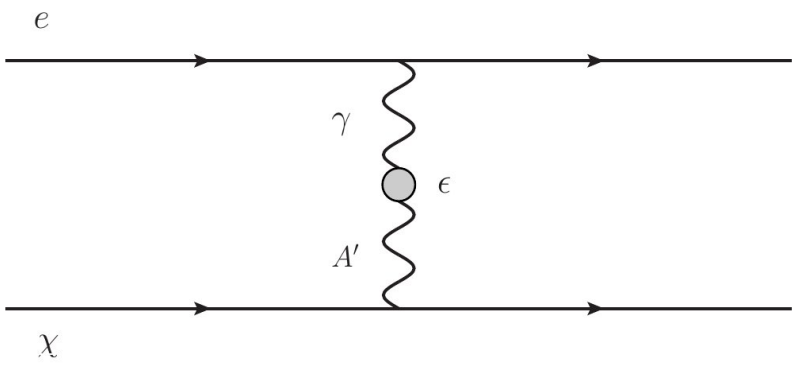

Figure 2.5: Feynman diagram for an interaction between SM electron and the particle χ from the hidden sector, charged under the new $U(1)'$ group. The interaction is mediated by the mixing of the SM photon and the DP. [5]

The main production channels of the DP are meson decays, proton bremstrahlung and QCD production. The main meson decays contributing to DP production are: [14]

$$\begin{aligned} \pi^0 &\to \gamma'\gamma \\ \eta &\to \gamma'\gamma \\ \omega &\to \pi^0\gamma \\ \eta' &\to \gamma'\gamma \end{aligned} \tag{2.10}$$

To calculate the differential production rate of DPs, the Weizsäcker-Williams approximation is used, see Ref. [15]. The DP decays by mixing with the SM photon, therefore

the sensitivity is proportionals to ϵ^2. Its decay width for decaying into leptons is given in equation 2.11 and its decay width into hadrons can be found in equation 2.12.

$$\Gamma(\gamma' \to l^+ l^-) = \frac{1}{3}\alpha_{QED} m_{\gamma'} \epsilon^2 \sqrt{1 - \frac{4m_l^2}{m_{\gamma'}^2}} \left(1 + \frac{2m_l^2}{m_{\gamma'}^2}\right) \tag{2.11}$$

$$\Gamma(\gamma' \to \bar{h}h) = \frac{1}{3}\alpha_{QED} m_{\gamma'} \epsilon^2 \frac{\sigma(e^+e^- \to \text{ hadrons})}{\sigma(e^+e^- \to \mu^+\mu^-)} \tag{2.12}$$

3 SHiP Experiment Setup

The SHiP experiment is currently under review by the relevant scientific committee at CERN (SPSC). For this reason this thesis will present the current status of research and development (R & D). It is planned to be located at the North Area of the SPS. The North Area shares the TT20 transfer line, which allows for slow extraction of protons from the SPS storage ring. Figure 3.1 gives an overview of the SPS and SHiP's planned location.

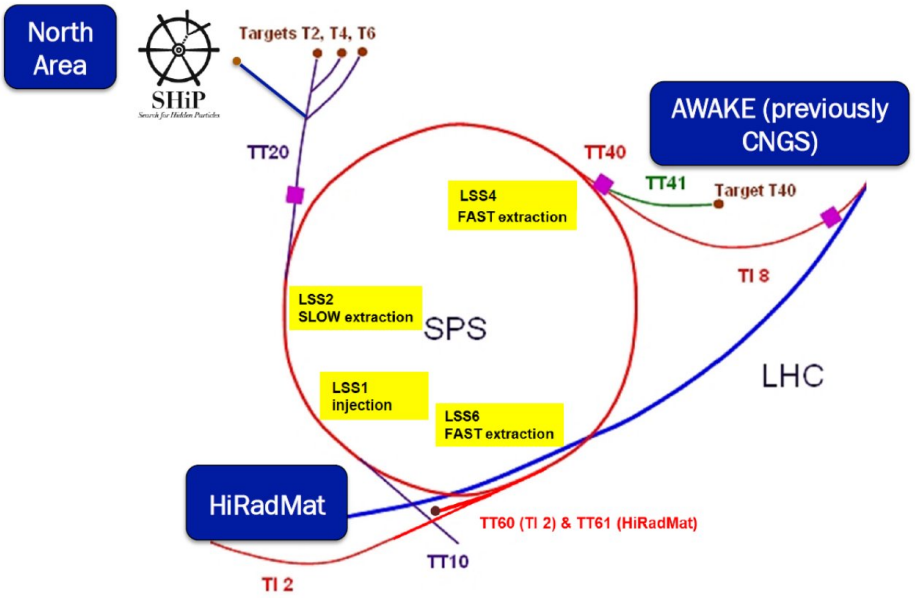

Figure 3.1: Location of the SHiP experiment in the North Area of the SPS [14]

Since SHiP is a new experiment at the intensity frontier, the beam intensity and consequently the Protons on Target (P.o.T) is pushed to the limits of the SPS. The beam intensity and the total P.o.T for the SHiP experiment has been estimated based on the five years of operation of the CERN Neutrino to Gran Sasso (CNGS) [16], assuming the current SPS running scheme with protons at 400 GeV. The actual energy will deviate from 400 GeV for about 5 GeV but this has a very small impact on the sensitivity studies, thus all studies were performed with a proton energy of 400 GeV. The TT20 would have to use a slow resonant extraction which would result in spills with a flat top of 1.2 seconds. It is realistic to assume that each spill contains $4 \cdot 10^{13}$ P.o.T. With some restrictions to the spill duration and the percentage of protons actually used for the SHiP experiment, the integrated flux would be $2 \cdot 10^{20}$ P.o.T over five years of data taking. [14]

3.1 Target

As discussed in section 2.1 the main production channel of HNLs are heavy mesons. For this reason the proton target needs to maximize the heavy meson production. The choice of a heavy target allows to reduce the number of (semi)-leptonic decays of pions and kaons, that would otherwise be by far the dominant source of muon and neutrino background. In addition to these challenging requirements, the target has to withstand a very high average beam power up to 350 kW deposited on the target, while the peak power during the spill amounts to 2.56 MW. To fit all requirements an extended study was performed and can be found in the Appendix A A.4 of Ref. [14]. Preliminary studies showed the feasibility of such a target with the following structure: a row of blocks of titanium-zirconium doped molybdenum (TZM), with a total length of four interaction lengths (58 cm) followed by six interaction length of pure tungsten (58 cm). A longitudinal cut of the target is shown in Figure 3.2.

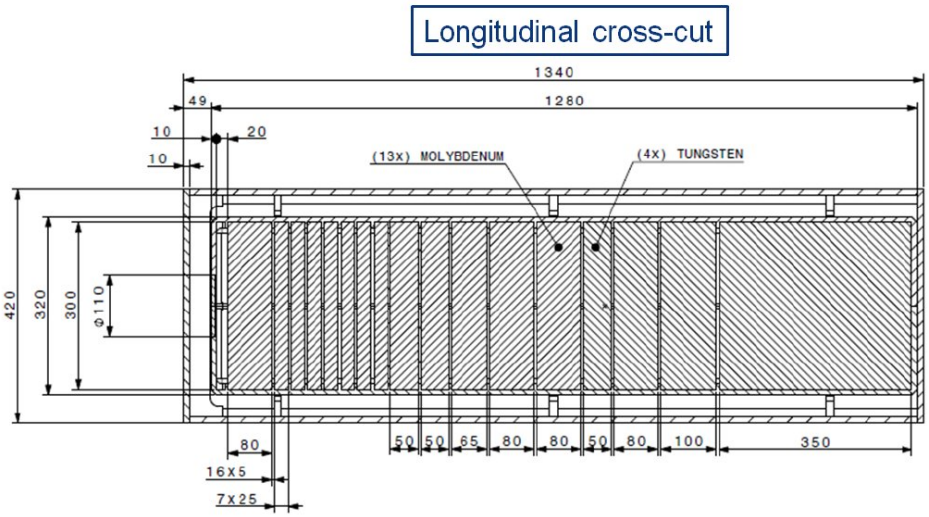

Figure 3.2: Longitudinal cross-cut of the proton target. The first 13 blocks are made out of TZM and the last four of tungsten. In between there are 5 mm slits for water cooling. Units are expressed in mm [14]

The blocks are cooled with water at 15 - 20 bar, so that the water boiling point is increased. The possibility of a cooling system based on gas is under investigation. The beam will impact an area of 30x30 cm^2 target with a longitudinal length of total 128 cm. [14]

3.2 Muonshield

With the current target design and a spill of $4 \cdot 10^{13}$ P.o.T about $5 \cdot 10^9$ muons are produced per spill. This number would lead to an unacceptable high rate in the detector and too large backgrounds. Therefore a muon shield, which reduces this flux

by many orders of magnitudes is needed. Based on simulation studies in Ref. [14] an active muon shield was chosen over a passive shield with heavy material, since the latter was not able to remove the most high energetic muons in less than 50 m. The momentum spectrum determines the design of the shield. Since the muons will have a momentum up to 350 GeV, a magnetic field of $B_y = 40$ Tm is needed to bend out the most energetic muons. The shield consists of two sections, the first section separates the μ^+ from μ^- and has a length of 19 m in z-direction (along the beam axis). The second section has a reversed field orientation to bend out muons, which are bent back by the return field of the first section. As it is visible in Figure 3.3 the second section ranges from 19 m to 48 m.

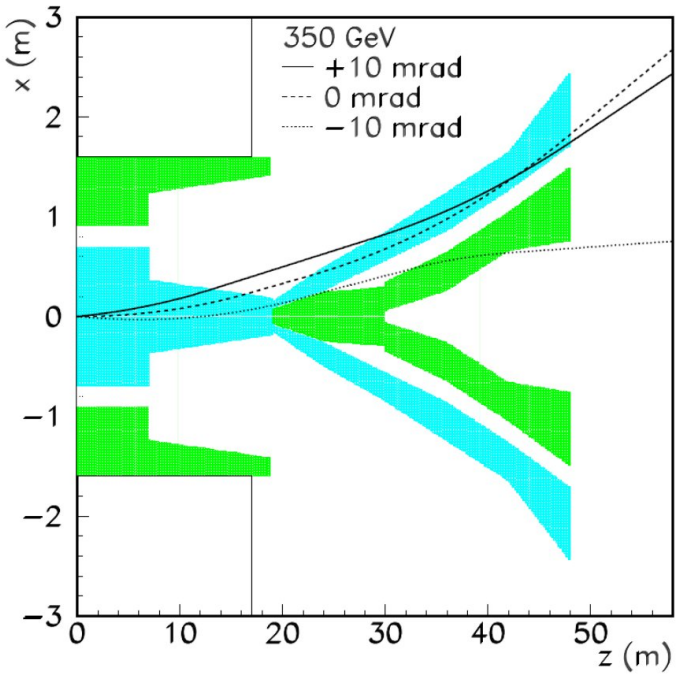

Figure 3.3: Schematic view of the active muon shield in x,z-plane. The different field orientations are shown in different colors (returnfield = green). The different lines represent muons with 350 GeV momenta and different opening angles with respect to the beam direction, at the beginning of the muon shield. [14]

Both section will consist of smaller magnets, each one around 6 m long. The cavern wall will have a minimum distance of 10 m from the target in the x-direction to minimize the number of muons back scattering into the decay volume.

3.3 ν_τ-detector

The ν_τ-detector consists of a neutrino target placed in a magnet (Goliath magnet from the H4 beam line at CERN) followed by Drift Tube Trackers and a magnetic spectrometer. An overview of the ν_τ-detector is given in Figure 3.4.

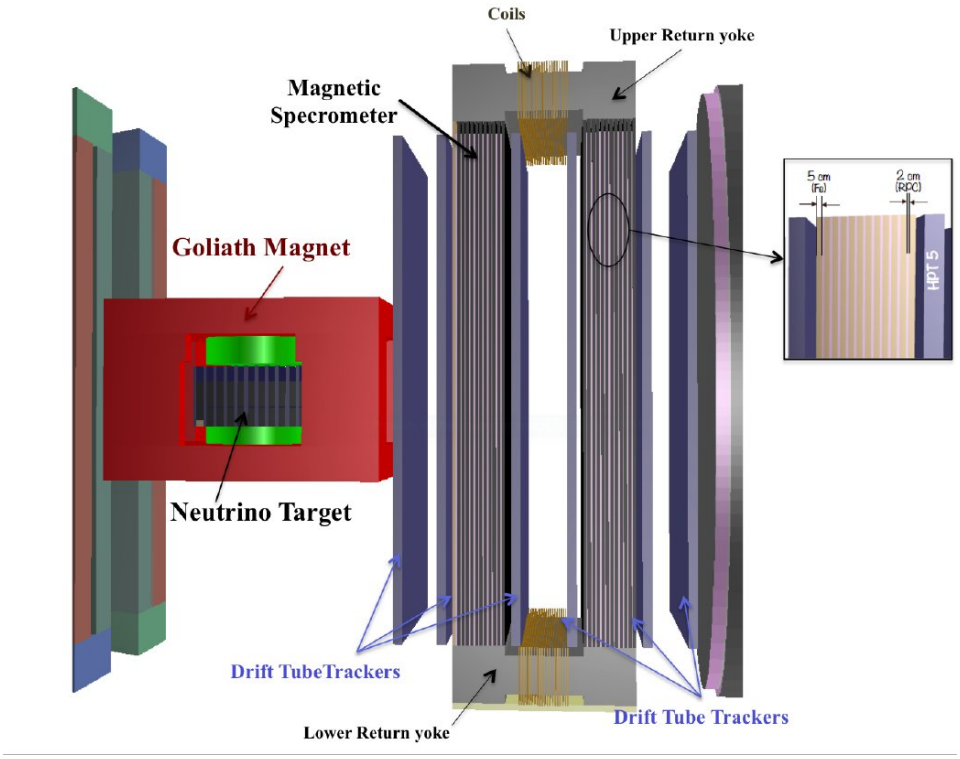

Figure 3.4: Overview of the ν_τ-detector [14]

3.3.1 Neutrino Emulsion Target

The neutrino target uses the Emulsion Cloud Chamber (ECC) technique. This technique employs a structure of alternating passive material with emulsion films. One unit cell (shown in Figure 3.5) consists of two parts, the ECC brick and the Compact Emulsion Spectrometer (CES). The CES uses a similar technique as the ECC brick but with light materials (e.g. Rohacell) as passive materials, while the brick has lead plates as a passive material.

Essential for the resolution of the neutrino target is the emulsion film used. These emulsion films consists of AgBr crystals scattered in a gelatin binder placed on both sides of a transparent plastic base. The crystals have a diameter of 0.2 μm and are sensitive to mimimum ionizing particles (MIP). The emulsion films have to be developed to enhance the growth of silver clusters (grains) for them to be visible by an optical microscope. A MIP particle leaves typically about 36 grains per 100 μm, which determines the sensitivity of the emulsion film. The angular resolution is in the milli-radian region and is measured by the distance of the grains of both sides of the plastic base of each film. One brick is made of 57 thin emulsion films interleaved with 56 lead plates of 1 mm thickness. The dimensions of the bricks are 128 (x) $\times$ 102 (y) mm^2 and 79 mm in z-direction. The full target consists of 11 walls of 15 $\times$ 7 bricks, while the walls are perpendicular to the beam direction and thus lying on the x-y plane. To ensure light-tightness, each brick will be packed in special aluminum-laminated

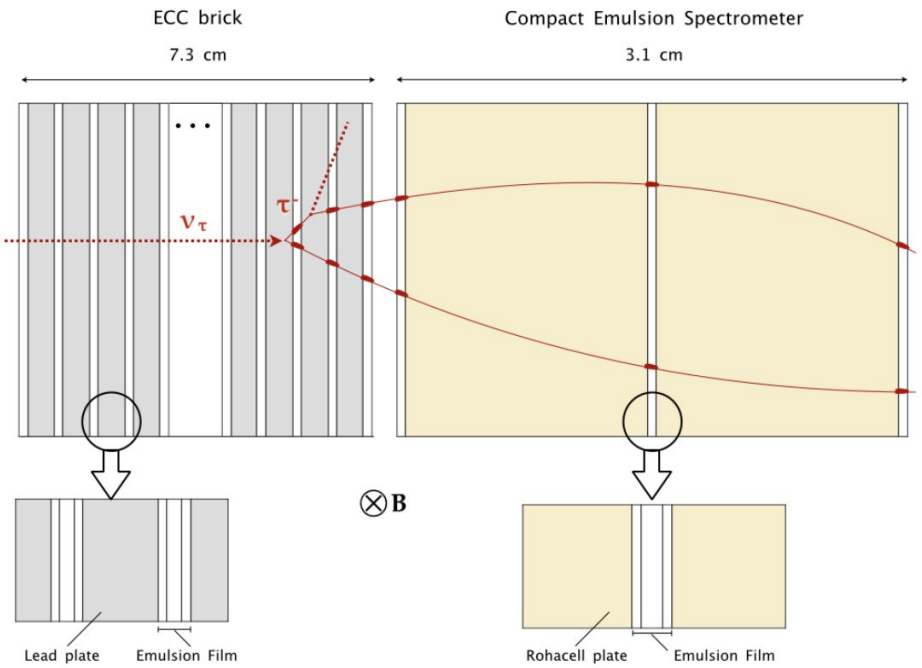

Figure 3.5: Schematic view of the unit cell of the neutrino emulsion target [14]

paper.

The purpose of CES is to measure the electric charge of the τ daughters. It is attached to the ECC brick and is made of three emulsions films with two intermediate layers of Rohacell, each with a thickness of 15 mm. The low density (Rohacell has a density of 57 mg/cm^3) of the passive material allows to minimize the multiple scattering inside the cell, in order to measure the magnetic deflection appropriately. The CES needs to be put under a magnetic field. It was found that the Goliath magnet is suited for this task. Its overall dimensions are $4.5 \times 3.6 \times 2.79$ m^3, the detailed design of the magnet can be found in Ref. [14]. The magnetic field has a cylindrical symmetry, with an approximately constant field inside the radius of the coils of the magnet. Outside the radius the magnetic field drops rather fast. The region with magnetic field of > 1 T determines a cylinder with a radius of $r = 1$ m (Figure 3.6).

The tracks are reconstructed and matched to the tracks from the neutrino target tracker (discussed in the section 3.3.2). Muons passing the bricks allow to measure the relative misalignment and thus sub-micron accuracy can be achieved.

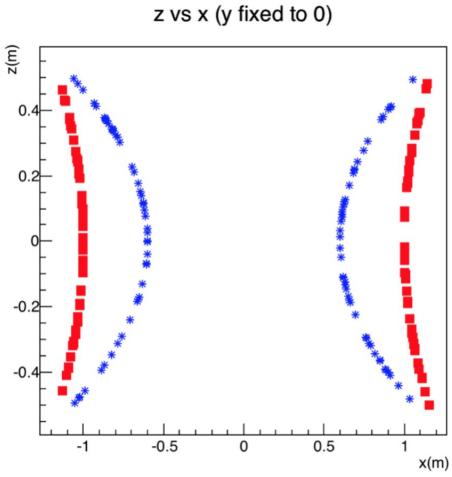

Figure 3.6: Behaviour of the magnetic field for the Goliath magnet. The red line marks the region which has a magnetic field above 1 T and the blue lines a field above 1.5 T [14]

3.3.2 Neutrino Target Tracker

As described in section 3.3.1 the neutrino target will consists of 11 walls and between each wall a Target Tracker (TT) plane is interleaved. In total 12 target planes will be needed, since one is placed upstream and will be used as a veto. For the TT, two different technologies are under study, scintillating fibers and a micro-pattern gas detector.

If scintillating fibers will be used, the detector will consists of so-called ribbons glued onto each other. One ribbon would consist of 5-6 layers of 250 μm fibers arranged as shown in Figure 3.7, glued together with epoxy bonding and impregnated with TiO_2. One TT module would consist of 7 ribbons placed in the horizontal direction and 15 ribbons in the vertical direction, placed orthogonally for best resolution. A ribbon for the horizontal direction would be 132 mm wide and 1980 mm long while ribbons for the vertical direction would have the same width and a length of 924 mm long. Additional to the ribbon layers, the module would consists of a closed-cell foam (e.g. Rohacell) or a honeycomb (e.g. Nomex) on which the ribbons are glued on, for stability reasons. The expected resolution for 6 layered ribbon is 70 μm. For the light detection SiPM chips would be used and directly connected to the readout side. Each ribbon would be read out by four 128-channel SiPM. The SiPM operates at temperatures of -40°C and needs thermal stability of $\pm$ 1°C.
Multiple options exists for gas detectors. In Ref. [14] the following are discussed: triple Gas Electron Multiplier (GEM), Micromegas and μ-RWELL. This thesis will only cover the concept of the GEM detector, since it is the most promising option at the moment. The cross section of a triple-GEM detector is shown in Figure 3.8. The GEM would be made of a 50 μm thin polyimide foil, with copper clad on each side of the GEM

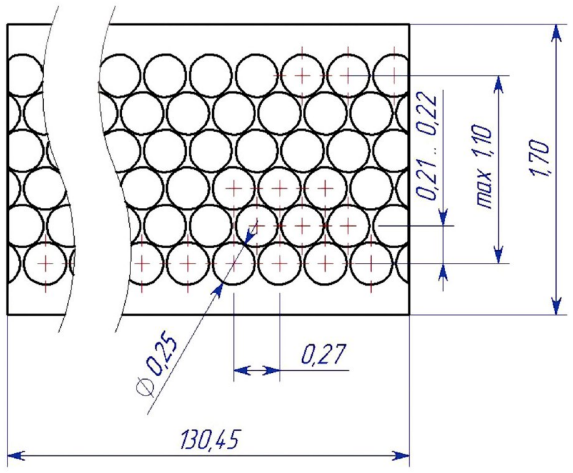

Figure 3.7: Ribbon cross section, units are in mm [14]

detector. The foil would be perforated with a high density of holes with each 70 μm diameter and a 140 μm pitch. Typically a voltage of 400 V would be applied leading to a field of 100 kV/cm within the holes. Triple staged GEM allow for a typical gain of the order of 10^4. For SHiP a foil with dimensions of 2 m $\times$ 1 m would be needed, but the largest foils produced are 200 cm long and 60 cm wide. To achieve the required dimension, two foils of 2 m by 50 cm are glued, with an overlap of 3 mm. The readout plane is a multi-layered circuit, patterned with a XY copper strips structure engraved at two different levels (labeled 2-D Readout in Figure 3.8).

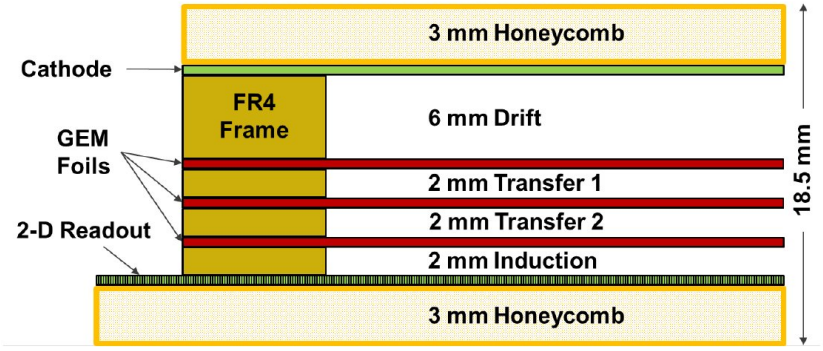

Figure 3.8: Cross section of a triple-GEM detector [14]

3.3.3 Muon Magnetic Spectrometer

The neutrino target will be followed by a muon magnetic spectrometer (shown in Figure 3.4) to identify muons produced in the τ decay from the neutrino target. The system is placed into a magnetic field to measure the momentum of the muons. The field is provided by a magnet with two vertical walls of rectangular cross section and which are connected by yokes at the top and the bottom. The total height of the magnet is 10 m (including the yokes) and it is 4 m wide to measure angles up to $\pi/4$.

Each wall consists of twelve iron layers of 5 mm thickness, interleaved with 2 cm of air for Resistive Plate Chamber (RPC) housing. The total thickness of the walls is 1.2 m. The RPCs are needed to track the muons inside the iron and the actual bending measurements are done by the drift tube tracker (discussed in section 3.3.4). The dipole magnet is magnetized by two coils, installed on the top and bottom yokes. These coils have 20 turns each and a current of 1.6 kA, which give an expected field of 1.75 T.

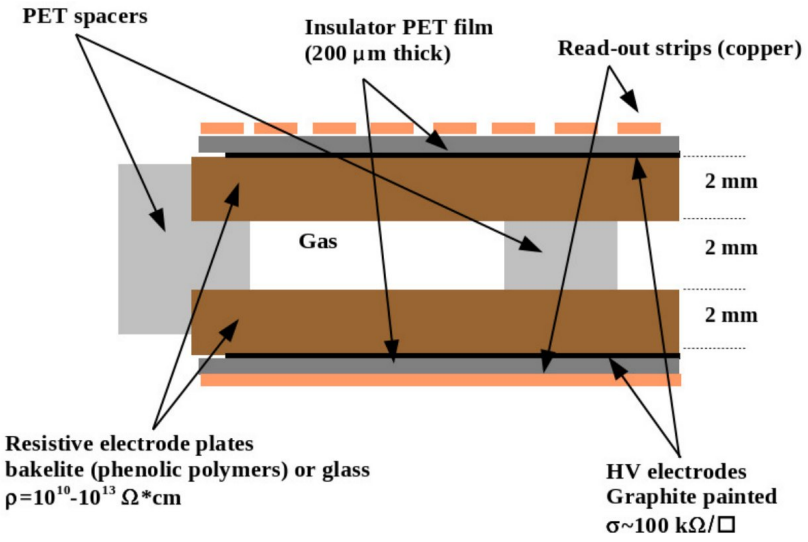

Figure 3.9: Cross section of a RPC with read out electrodes [14]

RPCs only require a resolution at a level of 1 cm. A cross section of a RPC detector is shown in Figure 3.9. The electrode plates are made out of 2 mm High Pressure Plastic Laminate, also known as bakelite and are painted with graphite for high surface resistivity. The graphite is isolated with 190 μm PET layers to maintain the space between the electrode plates. The readout strips are located on top of the cathodes. Different gas mixtures are at the moment under studies.

3.3.4 Drift Tube Tracker

The drift tube tracker is required for precise momentum measurements of the muon and its charge. To match tracks to those measured in the target, a 3D reconstruction will be needed. The drift tube planes are placed before, inside and after the muon magnetic spectrometer, as shown in blue in Figure 3.10. The stations before the muon magnetic spectrometer will consists of three planes each, with the second and third planes rotated by an angle of $\pm$ 3.6°. Each plane is made out of eight modules of each 48 aluminum tubes, arranged in four layers. The drift tubes are 7926 mm long and have an outer diameter of 38 mm, with a 0.85 mm wall. As a sense wire a 45 μm gold-plated tungsten wire is used. The total width of a module is 504 mm. A gas mixture of $Ar/CO_2/N_2$ is foreseen. To obtain a reliable time stamp a scintillating plane should be added just after the Goliath magnet as shown in yellow in Figure 3.10.

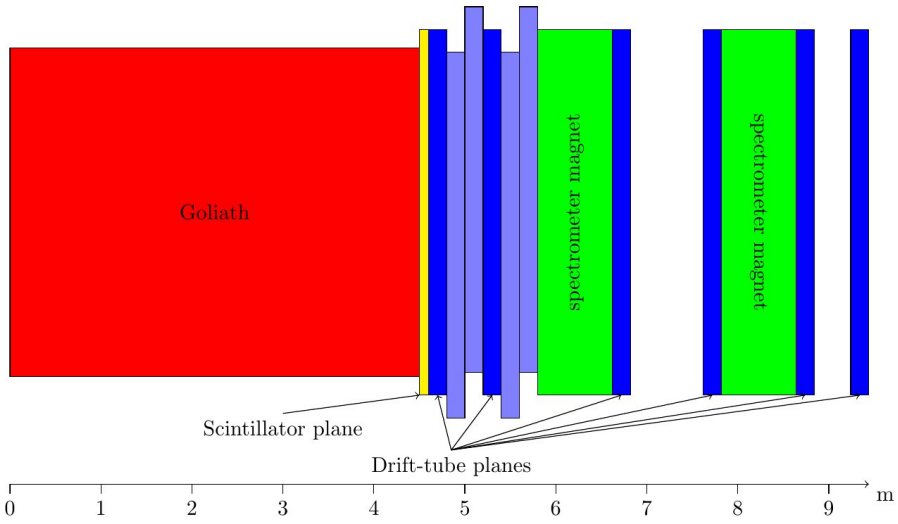

Figure 3.10: Top view of the ν_τ setup with the drift tube planes. The light blue drift tube planes are rotated by a stereo angle of $\pm$ 3.6°. [14]

3.4 The veto systems

To maximize the discovery potential of the experiment, the background rejection is essential. For this reason good veto systems are needed. The veto system consist of the following detectors and are also shown in Figure 3.13:

- Upstream Veto Tagger (UVT)
- Surrounding Background Tagger (SBT)
- Straw Veto Tagger (SVT)

HNLs will decay in the decay volume, showed in grey in Figure 3.13. To achieve a hermetic veto system, the vessel is double-walled and the space between the walls is filled with liquid scintillator. This veto system will be referred to as SBT.
The UVT is needed for particle detection from interactions inside the neutrino target (Neutrino Emulsion Target and Target Tracker in Figure 3.13) and consists of scintillating bars with wavelength-shifting (WLS) fibers to read out. It is placed in front of the decay volume. In order to reject K_S coming from the interactions of neutrinos with material before the decay volume, the SVT is located 5 m from the entrance window of the decay volume [14]. The three veto detectors are described below.

3.4.1 Upstream Veto Tagger (UVT)

The UVT consists of plastic scintillating bars, with WLS fibers that will be read out on both ends with a silicon photomultiplier. The scintillating bars are placed horizontally and are 4 m wide and 11 cm high. The total height of the detector is 12 m and the bars are placed with an overlap of 1 cm seen from the beam direction (shown in Figure

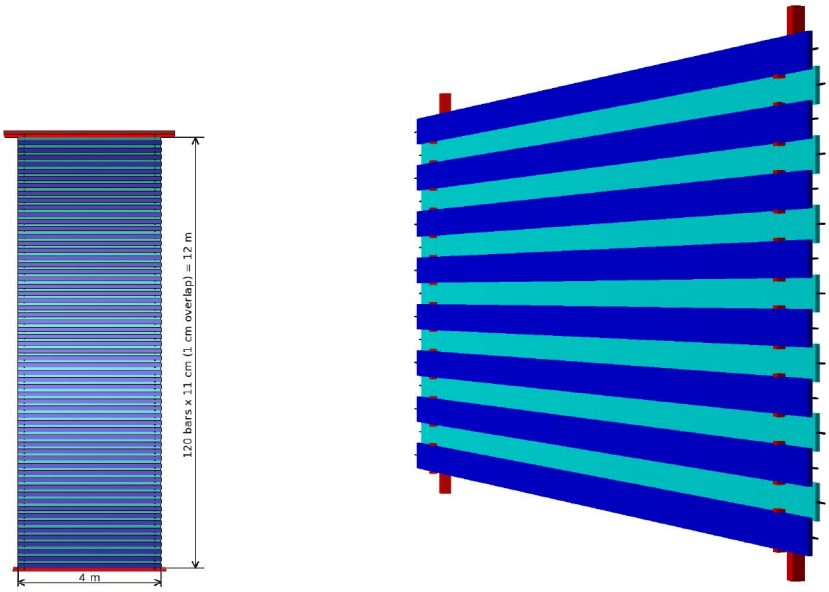

Figure 3.11: (Left) Schematic front-view of the UVT. (Right) Rotated 3D view of a section [14]

3.11). The time resolution of these bars is dominated by the decay time constant of the WLS fiber. Scintillating bars of 4 m length can achieve a time resolution of below 1 ns. [14]

3.4.2 Surrounding Background Tagger (SBT)

The SBT covers the surface of the decay volume with 30 cm thick liquid scintillator detector. The surface is divided in sections, which are 100 cm long in the z-direction and about 150 cm in the x and y direction and each section is read out with a Photodetector called WOM. In Figure 3.12 (a) a longitudinal cut of the HS vessel with the liquid scintillator section is shown. A WOM is a Photomultiplier tube (shown in Figure 3.12 (b)) with an attached tube, which is painted with WLS paint. The liquid scintillator

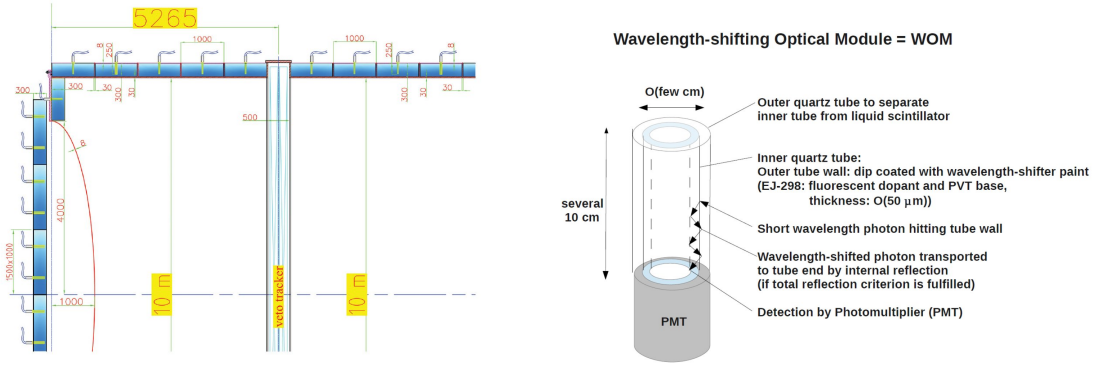

(a) Longitudinal cut of the vacuum vessel, first 8 m

(b) Schematic view of a WOM module

Figure 3.12: Schematic view of the HS vessel and the WOM module [14]

is a combination of the solvent linearalkyl-benzene (LAB) and 2,5-diphenyl-oxazole (PPO) which provides a good light yield with an emission spectrum maximum of 370 nm and a fast decay time. Also both components are widely available and can be purchased on large scales. [14]

3.4.3 Straw Veto Tagger

The SVT uses the same technology as for the spectrometer tracker, which is described in section 3.5.1. In comparison to the spectrometer tracker, the SVT will only consist of two views: one horizontal (Y) and one tilted by $\theta_{stereo} = +5°$ (U).

3.5 Hidden Sector Spectrometer

The decay volume is equipped with a spectrometer that provides momentum measurement and particle identification. The Hidden Sector Spectrometer consists of four tracking stations (discussed in section 3.5.1) including a magnet (discussed in section 3.5.2). Followed by an Electromagnetic Calorimeter (ECAL, discussed in section

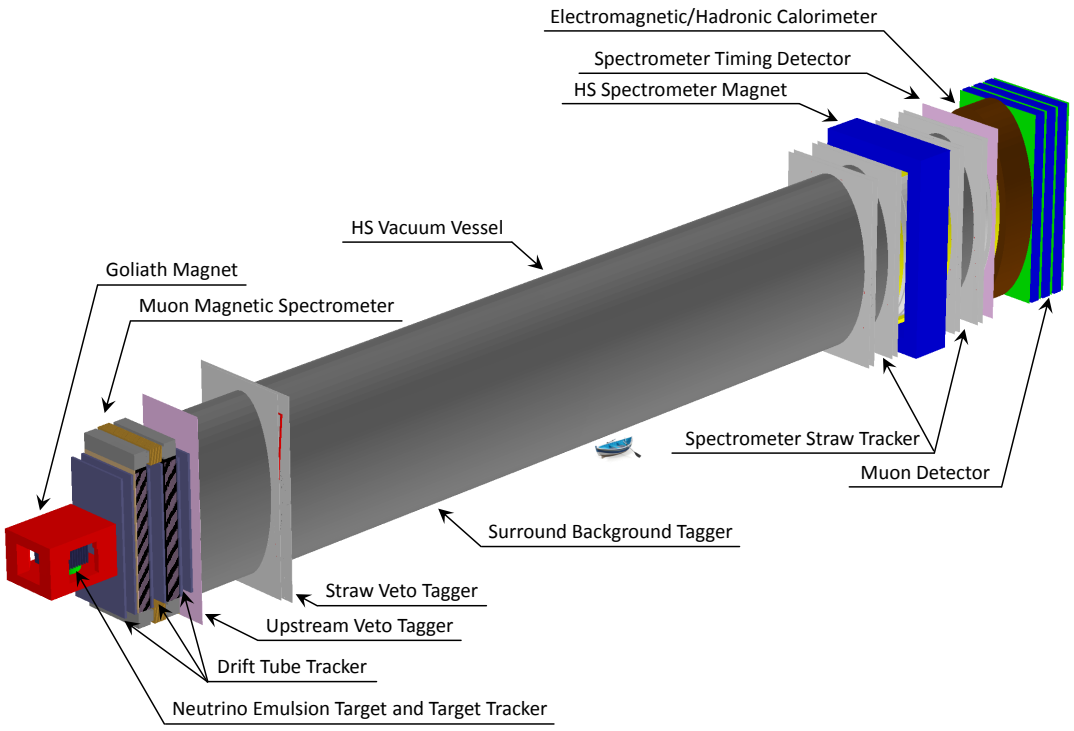

Figure 3.13: The SHiP detector layout including the veto systems and the ν_τ-detector [8]

3.5.3), a Hadronic Calorimeter (HCAL, discussed in section 3.5.4) and a muon detector (discussed in section 3.5.5).

3.5.1 Spectrometer Tracker

The spectrometer tracker uses the drift tube technology and consists of four tracking stations and a dipole magnet. The magnet (discussed in the section 3.5.2) is located in the middle of the four tracking stations and is 5 m long. The height of each station is 10 m and its width is 5 m. A tracking station has four views of which the first and the last one are oriented horizontally (Y) to measure the vertical coordinate. The planes in between are rotated by an angle of $\theta_{stereo} = \pm 5°$(U,V) so measure the transverse coordinate (X). In z-direction the first two and the last two stations are separated by a 2 m gap each and since the magnet is located between the second and the third station, the gap between those stations is 5 m. The outer (inner) diameter of the straws is 9.83

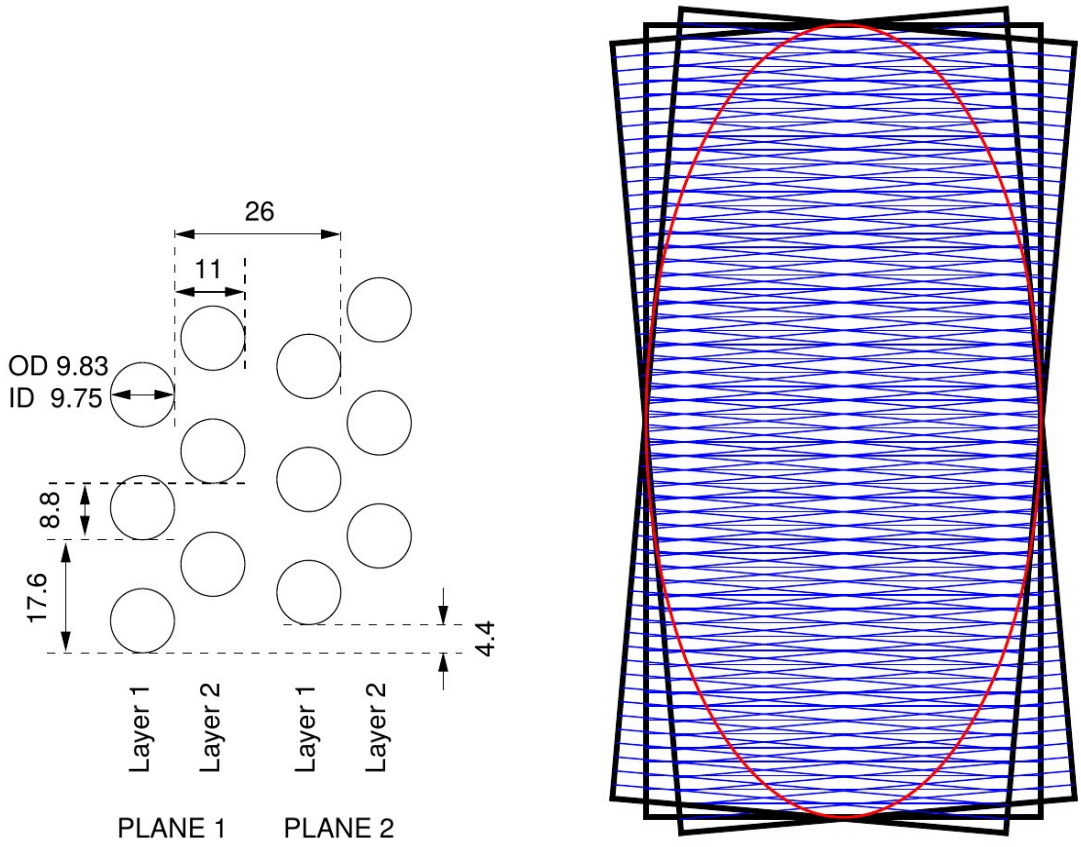

(a) Drift tube placement in one view of one tracking station

(b) Placement of the different views of one tracking station relative to each other

Figure 3.14: Cross section of a tracking station and relative placement of the different views [14]

mm (9.75 mm). Each view (shown in Figure 3.14 (b)) consists of two planes with each two Layers as shown in Figure 3.14 (a). The distance between the back of layer 1 and layer 2 is 11 mm in z-direction. The tubes in one layer have a pitch of 17.6 cm and the second layer is shifted vertically by 8.8 mm with respect to the first layer. Also Plane two is shifted vertically by 4.4 mm with respect to plane one. The drift tube

technology would be used to provide good spatial resolution and minimize multiple scattering. Long term tests (see NA62 [17] experiment) of straw trackers made out of thin polyethylene terephtalate (PET), showed that they are ideal to provide the desired properties. The straws proposed for the SHiP experiment are longer than for the NA62 experiment (5 m instead of 2.1 m), while the expected rate is lower.

3.5.2 Spectrometer magnet

The spectrometer magnet is needed to determine the momentum of the particles passing through the tracker. The momentum can be calculated from the bending of the tracks[3]. The absolute peak value of the magnetic field is 0.14 T and at the position of the nearest tracking station the absolute value is 0.08 T, thus negligible for the performance of the drift tubes. The design consists of two coils surrounded by a window-frame yoke structure. In Figure 3.15 the 3D schematic view of the magnet is shown.

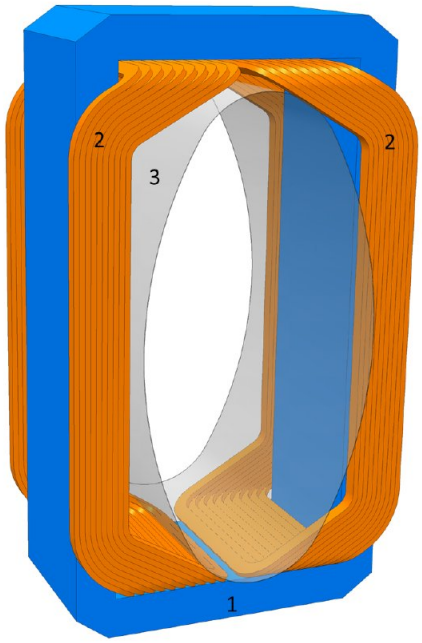

Figure 3.15: 3D view of the magnet (yoke (1) and coil (2)) with the HS vessel (3) [14]

The coil is made out of ten pancakes and each pancake consists of two layers with six turns each. The conductor of the pancake has a central hole (25 mm diameter) for water cooling. It is made out of Al-99.7 with a 50 x 50 mm^2 cross section.

[3] An alternative option with a magnetic field of 1 Tm is under study.

3.5.3 Electromatic calorimeter

The main task of the ECAL is to provide pion, photon and electron identification, measure the energy of photons and electrons (between 0.3 - 70 GeV) and provide timing information at ns level. The ECAL should also be able to reconstruct neutral pions in the energy range 0.6 - 100 GeV. The detector uses the shashlik technique, consisting of a scintillation-lead structure, where the scintillators are read out by WLS fibers. The shashlik technique uses blocks of detector material, which have WLS fibers distributed uniformly over each block. All the WLS fibers are guided to a photomultiplier tube. Each module (shown in 3.16) has 12 x 12 cm^2 transverse dimensions, which are read out in four section and thus each section has a transverse dimensions of 6 x 6 cm^2. A schematic view of the ECAL detector is shown in Figure 3.17. The ECAL covers a surface of 504 x 1008 cm^2 in the same elliptical shape as the decay volume (shown in Figure 3.13).

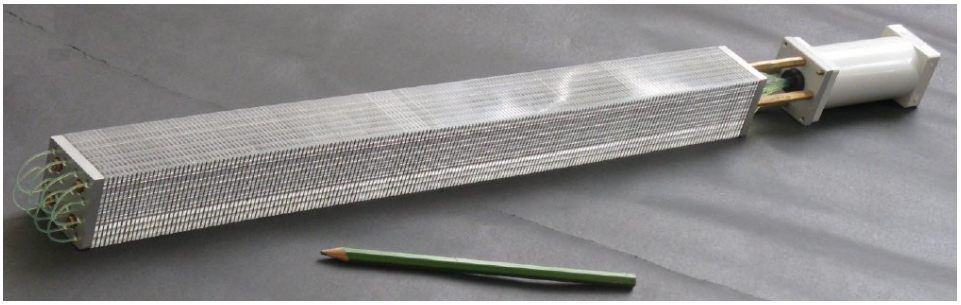

Figure 3.16: shashlik module [14]

3.5.4 Hadronic Calorimeter

The main goal of the HCAL is to provide pion identification and allow to tag neutral particles such as K_L and neutrons. It also provides timing information for background rejection.
For simplicity reasons, the same technique as for the ECAL was chosen for the HCAL. Instead of the full scintillator block, the HCAL module consists of alternating active (5 mm scintillator) and passive (15 mm iron) layers. As a preliminary solution two sets of modules are planned. The first set consist of 18 layers (seen as second layer in Figure 3.17) while for the second set 48 layers are foreseen (seen as third layer in Figure 3.17). This solution maximizes the discrimination between pions and muons at low momentum ($p < 5$ GeV/c). The modules have transverse dimension of 24 x 24 cm^2 and are also read out in 4 sections of 12 x 12 cm^2 each.

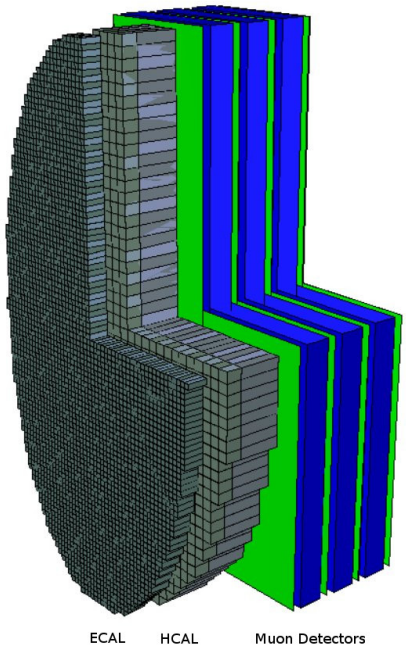

Figure 3.17: 3D position of the ECAL and HCAL with respect to the Muon Detector [14]

3.5.5 Muon Detector

The muon detector aims to provide muon identification. Examples of the signal decay channels with muon final states are: HNL $\rightarrow \pi^+\mu^-, \mu^+\mu^-\nu_\mu$. It is also used to separate the neutrino- and muon-induced background, mostly from $K_L \rightarrow \pi^\pm\mu^\mp\nu_\mu$ and $K_S \rightarrow \pi^+\pi^-$. In order to reach the muon system the particle needs a momentum of ~ 3 GeV/c. Below this momentum information coming only from the calorimeter can be used.

The detector consists of four active layers and three interjacent muon filters. Each layer is 6 m wide and 12 m high. The layout is shown in Figure 3.18. The active layers consists of scintillating bars which are supported with an aluminum structure. All active layers have horizontal and vertical strips. The strips consists of extruded plastic scintillator strips with WLS fibers and opto-electronic readout. The strips are 5 or 10 cm wide, depending on the granularity chosen, 3 m long and 2 or 1 cm thick. The needed granularity, driven by multiple scattering of the muon inside the system, was determined by studies based on MC simulation and was chosen to be in the range 5-10 cm in transverse direction. To construct the whole station 480 strips (of 5 cm width) are needed for each direction (horizontal and vertical). This results in 3840 strips and 7680 photodetectors in total. Several scintillating materials and WLS fibers are under study at the moment. The passive layer consists of iron walls, which are 60 cm thick and correspond to 3.4 nuclear interaction length. To reach the last muon station the muon need to have an energy at least 5.3 GeV/c^2.

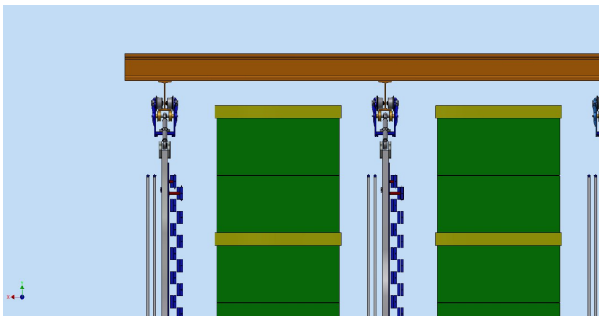

(a) Close up of the muon detector Layout

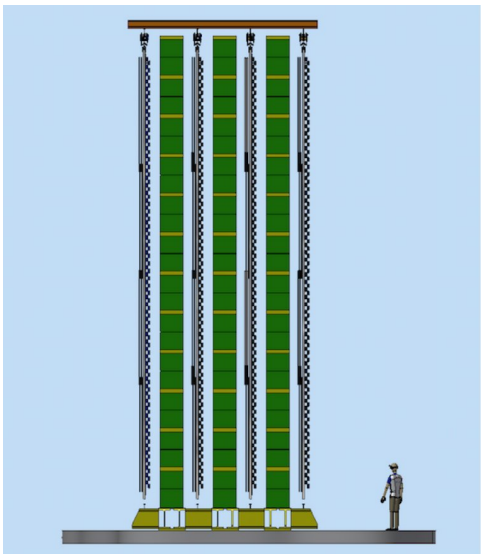

(b) Layout of the muon detector. The iron blocks are shown in green

Figure 3.18: Schematic views of the muon detector [14]

3.6 The FairShip simulation software

The software used in SHiP is called FairSHiP and is based on FairROOT, which is a package extending the software ROOT [18] used for data analysis and detector simulation. For simulation purposes the ROOT virtual Monte Carlo (VMC) was used to provide an interface to different transport engines. This allows the user code to be independent of the specific transport code. It provides several different Monte Carlo generators, like GENIE [19], PYTHIA8 [20], PYTHIA6 [21] and GEANT4 [22]. To simulate the detector, the TGEO package within ROOT was used. Several tools for reconstruction, analysis and visualization are provided within the FairROOT software. In addition FairROOT also provides tracks and geometry visualization.

Each simulation consists of two parts, the first part which simulates the proton-proton interactions and its decay products and the second part, which simulates the interactions of the products with the material. This is done separately for each background and for the HNL. The steps for the proton-proton simulation are the following:

1. The full facility complex is simulated, including the target, sweeping magnets, cavern, etc...
2. The proton-proton interaction is simulated with PYTHIA8
3. Corrections are applied for proton-nucleon scattering
4. The short lived particles are allowed to decay in PYTHIA8 while the long lived particles (i.e. pions, kaon, etc...) are passed to the second part

From the first part of the simulation, FairSHiP produces a spectrum of particles coming out of the thick target. For the neutrino-induced background the second part of the simulation consists of the following steps:

5. The neutrino spectrum is passed to GENIE, to simulate ν-proton interactions, both Neutral Current (NC) and Charged Current (CC)
6. These events are then passed to GEANT4 and distributed in the material surrounding the decay volume
7. Inside GEANT4 the detector response is simulated
8. Detector hits are passed to the FairSHiP reconstruction software which provides track candidate
9. The output of the reconstruction is passed to the analysis software which reconstruct signal candidtates.

The first part of the simulation is only done once and updated if the simulation of the facility is changed. The second part instead is repeated more often, since the reconstruction and detector response simulation are continuously improved.

4 Background sources

The signal signature consists of two isolated charged tracks fitting into a single vertex inside the fiducial volume. The fiducial volume, defined as the volume inside the decay volume between the SVT and the first tracking station, is the region where the background is best understood. Only HNLs decaying inside the fiducial volume can be distinguished from the background. In the decay volume the pressure is set to 10^{-6} bar to suppress neutrino scattering in the air to a level of 0.1 interactions in five years of data taking. The main background sources are:

- Neutrino inelastic scattering in the proximity of the decay volume
- Muon inelastic scattering in the proximity of the decay volume (either from the proton-target interactions or from cosmic muons
- Muon combinatorial background

The muon induced background is discussed inside this section, while the neutrino induced background, which is the main subject of this thesis will be discussed in section 5.

4.1 Cosmic muon background

The background from muons coming from the secondary cosmic rays is caused by inelastic scattering in the material surrounding the decay volume. The cosmic muon flux at sea level is 174 $m^{-2}s^{-1}$ [23]. We expect $3.2 \cdot 10^3$ muons to cross the detector during every spill, which results in $1.6 \cdot 10^{10}$ muons during the whole data taking period. The ratio of antimuons over muons is expected to be $N_{\mu^+}/N_{\mu^-} = 1.278$. To simulate this background, the events were generated in a large area of 30×90 m^2 above the experiment, with a flat momentum distribution. To correct the flat momentum distribution and the fact, that only around 10^7 events were simulated, an event-by-event weight was applied. It was found that the rate in the SBT is about 32 kHz. Events that leave an energy deposit of at least 45 MeV are vetoed by the SBT. This is the energy loss of a MIP going through 30 cm of scintillator. These events have an impact parameter (IP) to the target $>$ 33 m and thus are easily rejected by the offline analysis. More dangerous are the deep inelastic scattering (DIS) events coming from cosmic muons, for which a dedicated large statistic sample was produced. The number of expected DIS interactions is estimated to be:

$$N_{DIS} = \frac{\int N_\mu \cdot \sigma_{DIS}(p) \cdot N_{spills} \cdot \rho_{material} \cdot l \cdot \phi(p) dp d\Omega}{\int \phi(p) dp d\Omega} \tag{4.1}$$

Where N_μ is the number of incident muons per spill, N_{spills} is the number of spills during the experiment, $\rho_{material}$ is the mass density of the material in which the interaction occurred, l is the length of material passed by the muon and $\sigma_{DIS}(p)$ is the DIS cross section for muons and $\phi(p)$ is the momentum spectrum of the cosmic muons from [23]. The events were only simulated in the upper and lower experimental hall in the concrete walls, in the material of the vacuum vessel including the scintillator tank and the supporting ribs. Thus expected number of events in the different parts of the detectors are: [14]

$$\begin{aligned} N_{DIS}^{lower} &\approx 10.1 \text{ M events} \\ N_{DIS}^{upper} &\approx 10.1 \text{ M events} \\ N_{DIS}^{vacuum\ vessel} &\approx N_{DIS}^{inner} + N_{DIS}^{outer} \approx 3.23 \text{ M } + 0.31 \text{ M } = 3.54 \text{ M events} \end{aligned} \tag{4.2}$$

The muon DIS is simulated with PYTHIA6 and passed to Geant4 via the FairSHiP package (discussed in section 3.6). After applying the selection criteria (discussed in section 5.4), no events are left and leading to the background expectation shown in Table 4.1. The expected background is calculated by dividing 2.3 (mean of the Poisson distribution with the probability P($n_\nu \leq 0$) = 10 %) with the statistical weight. The statistical weight correspond to the ratio between the number of events generated and those expected in $2 \cdot 10^{20}$ P.o.T. To enhance the statistical power of the sample, factorization between the selection and veto is assumed.

Background source	Stat. weight	Expected Background (U.L. 90 % CL)
μ cosmics ($p < 100$ GeV / c)	2.0	1.2
μ cosmics ($p > 100$ GeV / c)	1600	0.002

Table 4.1: Upper Limit at 90 % CL on the cosmic muon background in two momentum ranges [24]

4.2 Muon combinatorial background

The muon combinatorial background arises from random combinations of muons which enter the decay volume and can mimic signal events. The muons enter the decay volume because of an imperfect muon shield or by back scattering from the surrounding cavern walls. With the FairSHiP full simulation the expected rate of reconstructed muons was estimated and found to be 7 kHz per spill, for momentum $p > 3$ GeV/c. For muons with a momentum $p > 1$ GeV/c a rate of 50 kHz is expected. A dedicated fast simulation was developed to evaluate the rejection of this background. In addition a sample consisting of two muons from different HNL decays was used to "fake" combinatorial background sample and a similar rejection was found for

this sample. Since these muons are randomly distributed over the whole spill length, the best way to remove this background is to require a coincidence between the two tracks. If $p_{\mu\mu}$ is the probability to find two muons in the same time interval $\Delta T =$ 340 ps with a muon rate $F = 7$ kHz, it is found that $p_{\mu\mu} \sim 1.4 \cdot 10^{-10}$. To calculate the number of combinatorial muons $N_{\mu\mu}$ in the five years of data taking, the probability has to be multiplied with the number of buckets, each containing $5 \cdot 10^6$ spills, the result is: $N_{\mu\mu} = p_{\mu\mu} \times N_{buckets} \simeq 2 \cdot 10^6$. These events can be rejected by requiring good vertexing and a rough pointing to the target. The expected background after offline selection is summarised in Table 4.2.

4.3 Muon inelastic scattering background

All muons deflected by the active muon shield will reach the cavern wall and interact with it. Particles produced in the muon inelastic scattering (mostly K_L, K_S, Λ) can get back to the decay volume. To simulate such events the muons were placed in the cavern walls with PYTHIA6. The simulation showed no background events from this type of interactions. In addition it is possible that some muons are not deflected enough with the active muon shield. These muons hit the material close to the decay volume and can mimic signal events. Assuming factorization between the veto of the incoming muon and the signal selection an additional suppression factor of 10^{-3} can be estimated, making this background negligible. The requirement to have no hits in the veto is sufficient to reject this background. This allows for an upper limit shown in table 4.2.

Background source	Stat. weight	Expected Background (U.L. 90 % CL)
μ combinatorial	-	0.02
μ inelastic	0.5	4.6

Table 4.2: Upper Limit at 90 % CL on the inelastic scattering muon background and combinatorial muon background [24]

4.4 SHiP sensitivity to HNL

To illustrate the SHiP potential to search for HNLs in the GeV scale, we use five benchmark scenarios. These scenarios are listed below, where normal (inverted) hierarchy of active neutrinos masses mean $m_3 > m_1, m_2$ ($m_3 < m_1, m_2$). The scenarios are:

I $U_e^2 : U_\mu^2 : U_\tau^2 \sim 52 : 1 : 1$, with inverted hierarchy [25]

II $U_e^2 : U_\mu^2 : U_\tau^2 \sim 1 : 16 : 3.8$, with normal hierarchy [25]

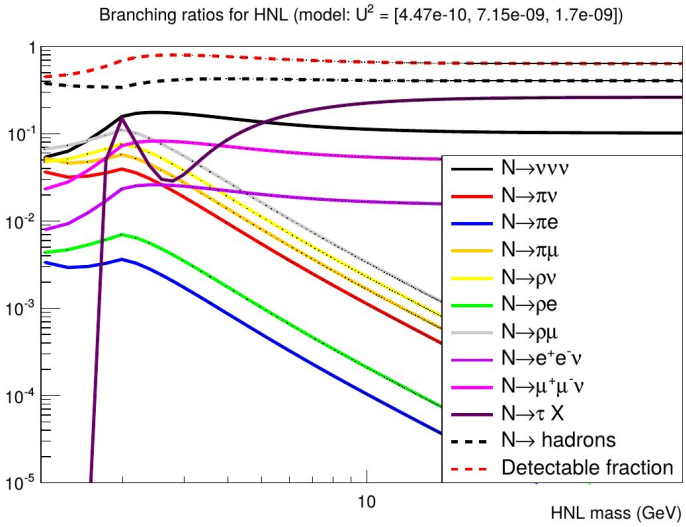

Figure 4.1: HNL branching ratios, as a function of the HNL mass, calculated for the scenario II with $U^2 = 9.3 \cdot 10^{-9}$. [14]

III $U_e^2 : U_\mu^2 : U_\tau^2 \sim 0.061 : 16 : 4.3$, with normal hierarchy [25]

IV $U_e^2 : U_\mu^2 : U_\tau^2 \sim 48 : 1 : 1$, with inverted hierarchy [26]

V $U_e^2 : U_\mu^2 : U_\tau^2 \sim 1 : 11 : 11$, with normal hierarchy [26]

Scenario II was used to generate events with the full simulation, with a total coupling of $U^2 = U_e^2 + U_\mu^2 + U_\tau^2 = 9.3 \cdot 10^{-9}$ and a HNL mass of 1 GeV/c^2. The results have been extrapolated to different couplings and different scenarios using a fast simulation, that was tuned with the full simulation. The number of HNL signal candidate observed in the experiment can be written as: [14]

$$n(\text{HNL}) = N(\text{p.o.t}) \times \chi(pp \to \text{HNL}) \times \mathcal{P}_{vtx} \times \mathcal{A}_{tot}(\text{HNL} \to \text{visible}) \qquad (4.3)$$

Where $N(\text{p.o.t}) = 2 \cdot 10^{20}$ the number of P.o.T, $\chi(pp \to \text{HNL})$ is the total HNL production rate, $\mathcal{P}_{vtx}$ the probability that the decay vertex is inside the fiducial volume of SHiP (defined in section 4) and $\mathcal{A}_{tot}(\text{HNL} \to \text{visible})$ is the detector acceptance of all visible final states.

The production rate $\chi(pp \to \text{HNL})$ takes into account the production of HNLs by charm and beauty mesons. The main production of HNL comes from D_s and B_s meson decays as seen in equation 2.4 [27].

To calculate the probability $\mathcal{P}_{vtx}$ the HNL lifetime was used, which is calculated by adding all decay channels[4] (listed in equations 2.6, 2.7). The expected branching ratios are shown in Figure 4.1.

The quantity $\mathcal{A}_{tot}(\text{HNL} \to \text{visible})$ is defined as follows:

[4] Decays such as HNL $\to 3\nu$ are considered in the calculation of the HNL lifetime, but of course are not included in the visible branching ratios

Selection	Entries	Acceptance	Rel. loss [%]
Full sample	1065	9.07e-05	-
Geometric Acceptance	430	1.93e-05	74
Straw 1 and 2	259	7.47e-06	61
Straw 4	221	5.78e-06	23
ECAL	221	5.78e-06	0
Muon Station 1	217	5.65e-06	2
Muon Station 2	214	5.55e-06	2

Table 4.3: Acceptance for various selection requirements for the decay channel HNL $\rightarrow \mu\pi$ and the scenario II and a total coupling of $U^2 = 9.3 \cdot 10^{-9}$. The different selection are defined as follows: "Geometric Acceptance" requires the vertex to be between the entrance window and the exit window of the vessel and it also demands that the x and y position of the vertex lies in the ellipse, defined by the decay volume. "Straw 1,2,4" is needed to ensure, that the daughter particles leave tracks in the straw stations and "ECAL" is needed to distinguish some channels (e.g. HNL $\rightarrow \mu\pi, ee\nu$). If the channels has some muons in the final state (e.g. HNL $\rightarrow \mu\pi, \mu\mu\nu$) , the muon stations also need to register some hits. This is ensured with the selections "Muon station 1,2".

$$\mathcal{A}_{tot}(\text{HNL} \rightarrow \text{visible}) = \sum_{i=\text{visible channel}} \mathcal{BR}(\text{HNL} \rightarrow \text{i}) \times \mathcal{A}(\text{i}) \tag{4.4}$$

with $\mathcal{A}(i) = \frac{\#\text{ reconstructable}}{\#\text{ simulated}}$ being the acceptance for the detectable final state i and $\mathcal{BR}(\text{HNL} \rightarrow \text{i})$ the corresponding branching ratio. Detectable channels are considered HNL decays with at least two charged particle in the final state, including decays such as HNL $\rightarrow \rho^0\nu$, with$\rho^0 \rightarrow \pi^+\pi^-$. Decays such as HNL $\rightarrow \pi^0 + ...$ are considered indistinguishable from the background and are not included in the estimate of the sensitivity.

The acceptance for the "golden" mode HNL $\rightarrow \pi\mu$ and for the couplings defined as in scenario II, is shown in Table 4.3. More studies have been performed with different masses and couplings can be found in Ref. [14].

In addition to the acceptance, summarized in Table 4.3, selection criteria are applied to reject the background. These are discussed in details in section 5.4. The sensitivity of the SHiP experiment for the scenarios introduced above, including the selection efficiency, is illustrated in Figure 4.2 - 4.3.

The grey area is ruled out by requiring that the HNL explain the BAU and are consistent with neutrino oscillation experiments. Constraints from previous are shown by the green curves. The sensitivity of the SHiP experiment can improve by several orders of magnitudes to present constraints below a mass of 5 GeV/c^2 and in particular below the mass of charm mesons (2 GeV/c^2), allowing to probe for the first time the cosmological most interesting region.

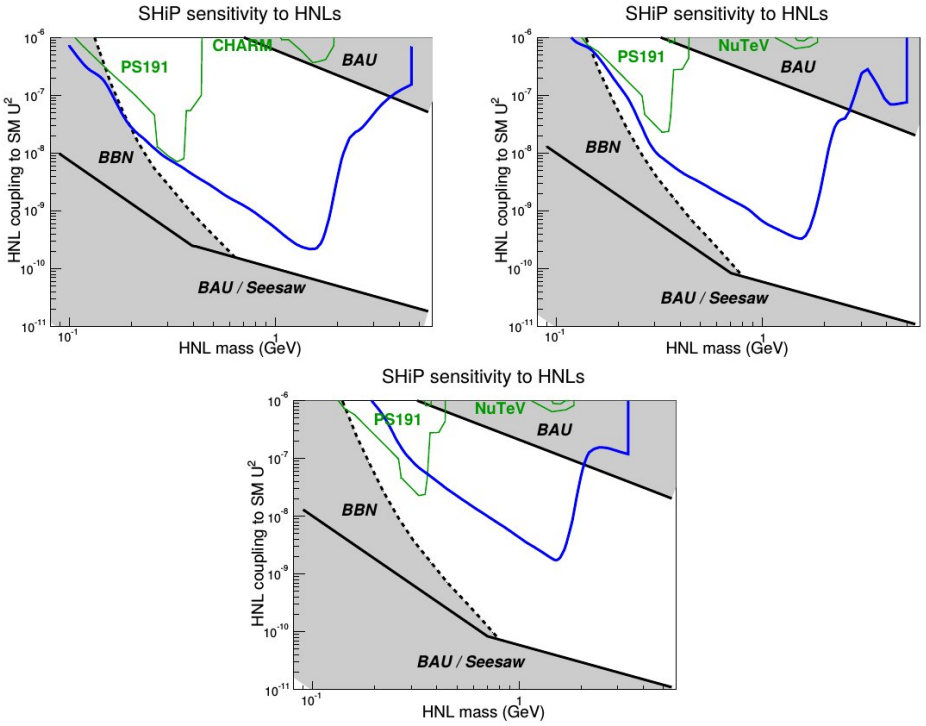

Figure 4.2: Sensitivity to HNL for the scenarios I, II and III, where U_e^2, U_μ^2 and U_τ^2 dominate respectively. [14] The grey regions corresponds to constrains from the Big Bang Nucleosynthesis, the requirement that the HNL explain the BAU and measurements of neutrino oscillations. The experimental constraints correspond to 90 % CL upper limit. The green curve are the best limit from previous experiments, while the blue curve is the expected upper limit at 90% CL of the SHiP experiment with $2 \cdot 10^{20}$ P.o.T.

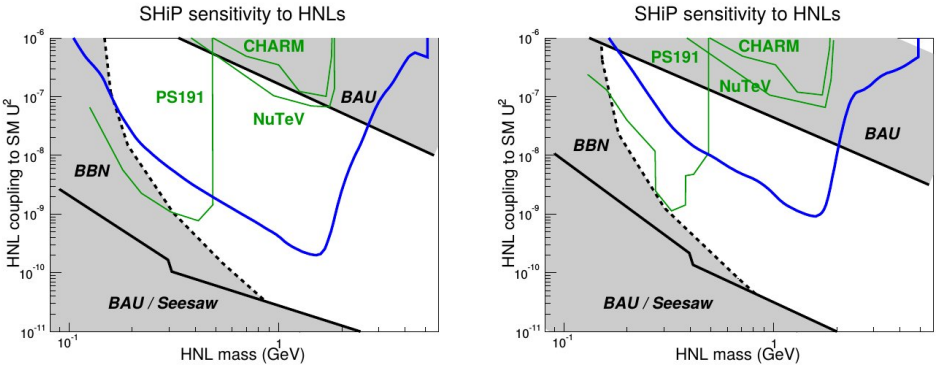

Figure 4.3: Sensitivity to HNL for the scenarios IV and V. [14] The grey regions corresponds to constrains from the Big Bang Nucleosynthesis, the requirement that the HNL explain the BAU and measurements of neutrino oscillations. The experimental constraints correspond to 90 % CL upper limit. The green curve are the best limit from previous experiments, while the blue curve is the expected upper limit at 90% CL of the SHiP experiment with $2 \cdot 10^{20}$ P.o.T.

4.5 Dark Photon sensitivity

The sensitivity of the SHiP experiment to DP is calculated with a similar method as the one discussed for HNLs. Instead of the full simulation a dedicated fast simulation was used. PYTHIA8 was used to generate DP produced from mesons decays, while theoretical calculations [5, 28, 29] are used to generate DP coming from proton bremsstrahlung and QCD production. The geometrical acceptance is calculated with the fast simulation, which was tuned with the full simulation. The detector reconstruction efficiency and the selection has been studied with the full FairSHiP simulation. The results are shown in Figure 4.4.

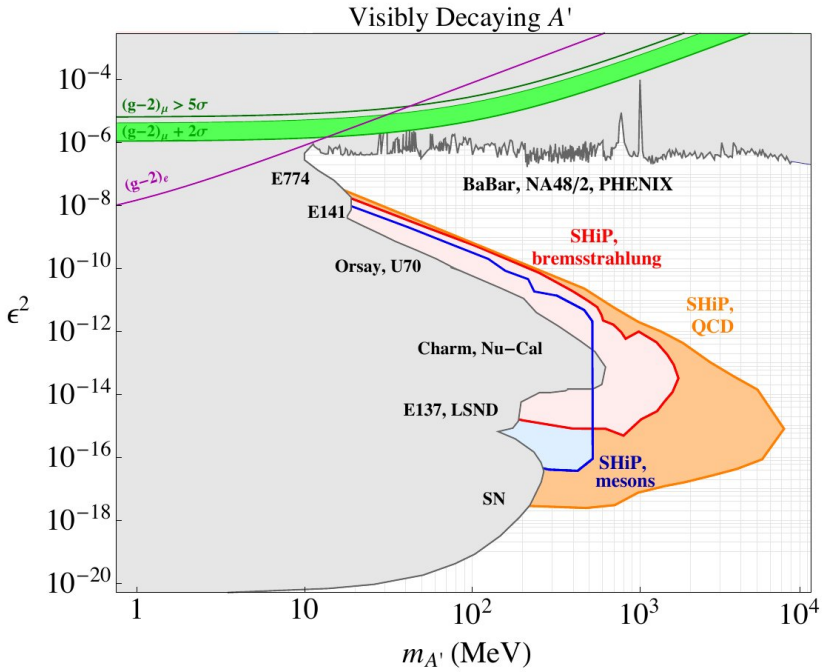

Figure 4.4: Sensitivity for dark photons, the different production channels (mesons, proton bremsstrahlung and cascade production) are shown separately. [24] Sensitivity to the DP from past experiment compared to the expected SHiP constraints. The grey area correspond to upper limit 90 % CL from previous experiments. The blue, red and orange region are limits on 90 % CL that SHiP can set for different production mechanism of the DP.

5 Analysis Methods

Neutrinos interacting in the vicinity of the decay volume can produce particles that enter the decay volume and mimic the signal. To distinguish between the background and the signal, several veto criteria are used in addition to selection requirements. The background rejection is studied in this section and an estimate of the expected background yield in $2 \cdot 10^{20}$ P.o.T, corresponding to five years running at nominal conditions, is given.
The pressure of 10^{-6} bar in the decay volume of the current experimental set up, has been determined by requiring to have less than one neutrino interaction with the air molecules in the decay volume in five years of data taking. This requirement is very conservative since reconstruction capability as well as selection criteria are expected to significantly reduce this background. In this section we present a study of the neutrino background at atmospheric pressure. The possibility to relax the pressure requirements would have a big impact on the experimental design and would allow to significantly reduce the cost. The studies to analyze the possibility to reduce the required pressure, and therefore to reduce the detector costs, are also presented in this section.
The main results are the estimate of the expected number of background events, which are presented in section 6.

5.1 Studies of neutrino scattering in the vicinity of the decay volume

The neutrino interaction is generated with GENIE, taking as input the neutrino momentum determined with FairSHiP (shown in Figure 5.1). The proton-nucleon interaction in the target is simulated with PYTHIA8, which is also used to make short living particles decay. Particles are passed to GEANT4 which simulates the interaction with the material. Neutrinos mostly come from decays of pions and kaons, which are not absorbed by the target, and by decays of heavier mesons such as charm. For this thesis only muon neutrinos were produced since they are the dominant neutrino background (coming from decays of pions and kaons).
To maximize the statistical power of the sample, the trajectory of each neutrino is re-used several times. Each event, defined as the interaction of the primary neutrino, is weighted according to the material density that the neutrino sees in his trajectory:

$$weight = \frac{\rho \cdot L \cdot N_A \cdot N_{nu} \cdot \sigma}{N_{generated}} \tag{5.1}$$

Where ρ is the mean material density seen by the neutrino, L the length of the neutrino path, N_A the Avogadro number, N_{nu} is the number neutrinos expected from the

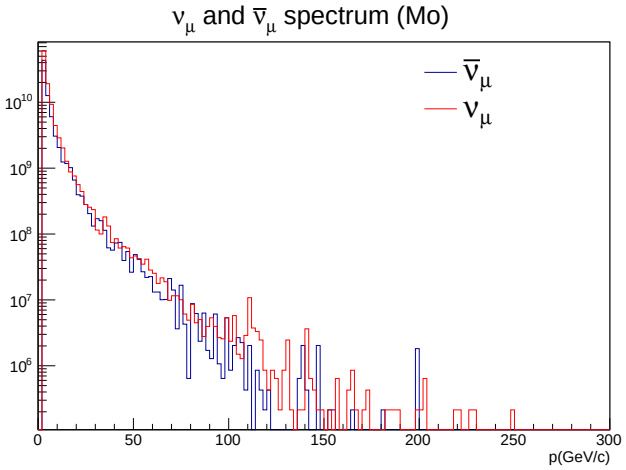

Figure 5.1: Momentum spectrum for ν_μ (red) and $\bar{\nu}_\mu$ (blue) after the absorber. The mean momentum is 5.54 GeV/c for ν_μ and 5.738 GeV/c for $\bar{\nu}_\mu$

number of P.o.T, σ the energy dependent cross section and $N_{generated}$ is the number of generated events. In order to enrich the statistics in a particular region of the phase space, several samples have been produced, as shown in Table 5.1. The weights have been recomputed for each production to ensure that the normalization is correct.

Name of the Production	# generated events (ν,$\bar{\nu}$)	Energy range (ν,$\bar{\nu}$)
Sample 1	$(1.533 \cdot 10^7, 1.75 \cdot 10^6)$	2 - 100 GeV (both)
Sample 2	$(1.0 \cdot 10^7, 2.0 \cdot 10^7)$	(2-10 GeV, 2-200 GeV)
Sample 3	$(1.484 \cdot 10^8, 1.589 \cdot 10^8)$	2 - 100 GeV (both)

Table 5.1: Summary of the samples generated for the study of the neutrino background

A sample of anti-neutrinos has also been produced with the same methods. The expected number of anti-neutrinos is roughly $N_{\bar{\nu}} \sim 3 \cdot 10^{17}$ while the number of neutrinos is expected to be $N_\nu \sim 4 \cdot 10^{17}$, while the cross section of neutrinos is about twice as large as that of anti-neutrinos. This results in $\sim 10^7$ expected neutrino interactions in the experimental set up.

-	Total number generated	Reconstructed events	events/ 5 years
neutrino	$1.754 \cdot 10^8$	890709	35049.1
anti-neutrino	$1.791 \cdot 10^8$	599405	11225.2

Table 5.2: Summary of the neutrino background samples generated in the full momentum region 2 - 100 GeV. The first column indicates the number of generated events, the second column the number of neutrino events with at least two charged particles in the HS spectrometer and the third column gives the expected number of reconstructed events if five years of running.

5.2 Studies of neutrino scattering inside the decay volume

The sample dedicated to study the neutrino interactions inside the decay volume filled with air at atmospheric pressure, was produced with the same methods for the neutrino interactions in the vicinity of the decay volume. To only produce events inside this volume, three modifications to the FairSHiP software had to be done:

1. replace the vacuum with air at atmospheric pressure inside the cave geometry
2. set the z-range of the interaction point to fit the fiducial volume (end of straw veto position + 20 cm to beginning of first tracking station - 20 cm)
3. reset the x/y constraints inside GENIE to match the elliptical shape of the decay volume (-1cm for each semi-major/minor axis)

From the mean energy of the input spectrum (shown in Figure 5.1) and an average path of 50 m of air at atmospheric pressure, the expected number of neutrino interactions is $1 \cdot 10^5$ during 5 years of data taking[5].

-	Total number generated	Reconstructed events	events/ 5 years
neutrino	$2.0 \cdot 10^5$	7704	1959.3
anti-neutrino	$2.0 \cdot 10^5$	8600	1132.7

Table 5.3: Summary of the statistic of the sample for neutrinos interacting in the decay volume

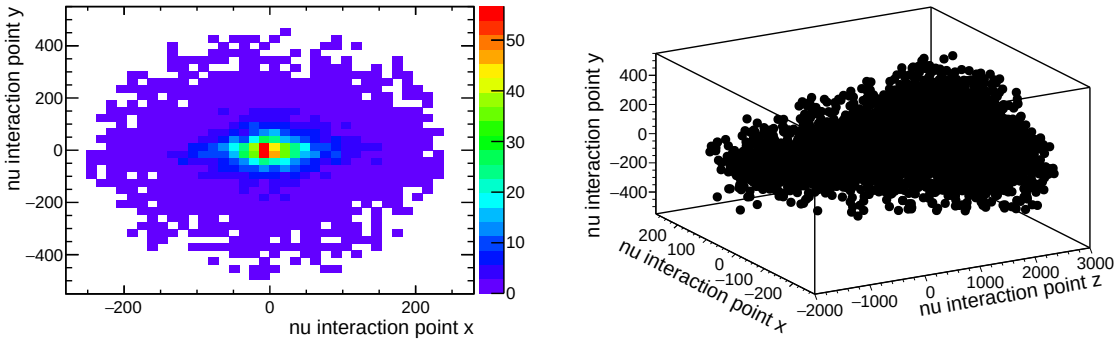

(a) True MC position of the ν interaction in the xy plane

(b) True MC position of the ν interaction in the 3D-space

Figure 5.2: True MC position of the interaction for reconstructed neutrino events in the air sample

[5] The number of expected neutrino interactions in 50 m of air was calculated with the following formula: $N_{\text{interactions}} = \rho \cdot L \cdot N_A \cdot N_{nu} \cdot \sigma$, where σ is the cross section, $N_{nu} = 4.2 \cdot 10^{17}$ the number of neutrinos produced in SHiP, N_A the Avogadro constant and ρ the air density and $L = 50$ m the average neutrino path through the air. For anti-neutrinos about half of the events are expected, since the cross section is about half of the neutrino cross section.

Two samples for neutrino and anti-neutrino interactions, each corresponding to $2 \cdot 10^5$ events, were produced (the summary is given in Table 5.3). To confirm that the interaction only take place inside the fiducial volume, the true MC positions of the neutrino interaction are shown in Figure 5.2.

5.3 Kinematical Studies

In order to optimize the selection the kinematic properties of the particles originating from neutrino interactions have been studied. Particular attention was given to neutral particles, that can not be vetoed and long lived particles, such as K_0, which can enter the decay volume and mimic the signal signature.

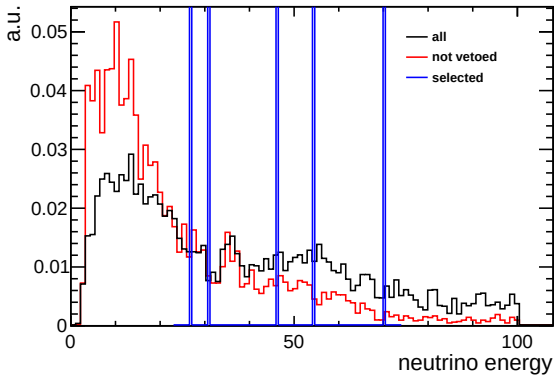

(a) Neutrino energy distribution

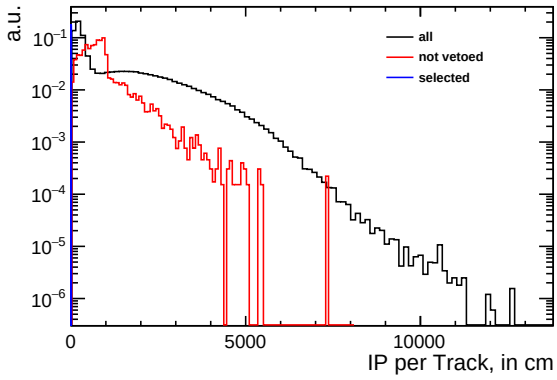

(b) IP distribution

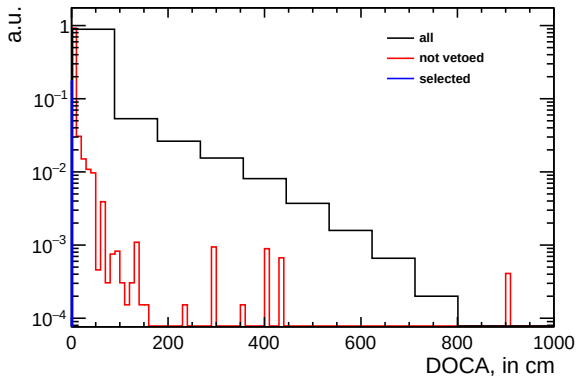

(c) DOCA distribution

Figure 5.3: Kinematic studies of the neutrino interactions in the currently proposed, evacuated experimental set up

In Figure 5.3 (a) the energy distribution of the primary neutrino is shown. As it was already mentioned, the sample was produced to energies up to 100 GeV, starting from energies of 2 GeV to exclude elastic scattering. As expected from the input momentum spectrum, the lower energies are more frequent than higher energetic neutrinos. In the same Figure also the distribution is shown for the events surviving the veto systems

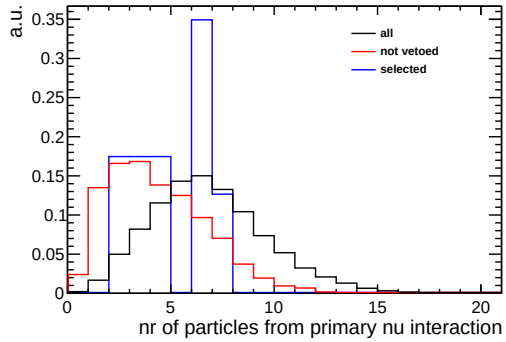

(a) Distribution of the number of particles produced by the primary neutrino

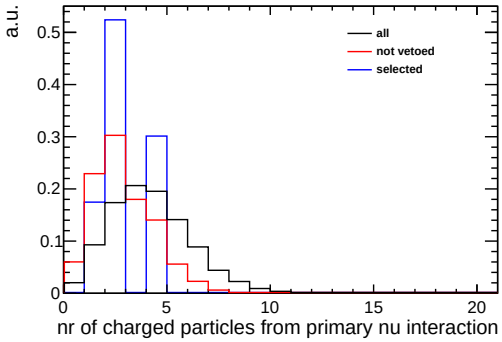

(b) Distribution of the number of charged particles produced by the primary neutrinos in an event

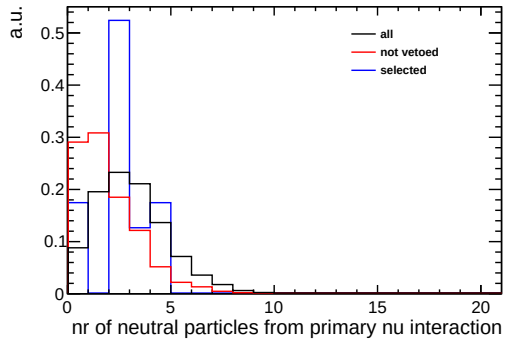

(c) Distribution of the number of neutral particles produced by the primary neutrinos in an event

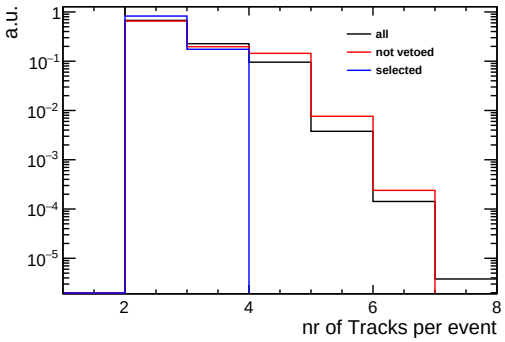

(d) Number of tracks per primary neutrino interaction

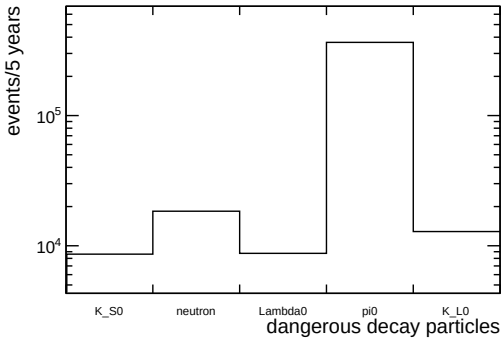

(e) Expected yield of neutral particles in five years of data taking produced by inelastic neutrino interaction

Figure 5.4: Study of the different type of particles produced in neutrino interactions in the current experimental setup

and selection criteria (discussed in the next section). Neither the selection nor the veto system reject a special energy range.
In Figure 5.4 (a) the total number of particles produced by the primary neutrino is shown. It shows that all of the events have < 15 particles and the selection as well as the veto system reject the events with high multiplicity. Figures 5.4 (b) and (c) show the number of charged and neutral particles produced by the primary neutrino. The veto system again reject events with high multiplicity and the selection criteria selects events with < 5 neutral or charged particles.
In Figure 5.4 (e) the yield of the most dangerous neutral particles, such as $\pi^0, \Lambda_0, K_L, K_S$ and n, is shown. While the yield is dominated by neutral pions, the most dangerous background consists of V_0 particles such as Λ_0 and K_0 which can decay and mimic the experimental signature of HNLs. These are more dangerous than others, because their decay products have a similar or even the same signature as the HNL decay. To compare the decay channels of the dangerous particles with the ones from the HNL (listed in equation 2.6 and 2.7) a list of the most dominant channels is shown in equation 5.2.

$$\begin{aligned}
&\Lambda_0 \to p + \pi^-, n + \pi^0 \\
&\pi^0 \to 2\gamma, e^+e^- \\
&K_L \to 3\pi, \pi^\pm + \mu^\mp + \nu_\mu, \pi^\pm + e^\mp + \nu_e \\
&K_S \to 2\pi^0, \pi^+\pi^-
\end{aligned} \tag{5.2}$$

In Figure 5.4 (d) the number of tracks per event in the tracking station is shown. Events with < 2 tracks are rejected at the reconstruction level because the signal signatures consists of at least two tracks. The veto system in general events with high-multiplicity of particles in the neutrino interaction point, in addition the selection requires isolated tracks fitting into a vertex.
Important discriminating variables to distinguish the signal from the background are the Impact Parameter to the target (IP) and the Distance of Closest Approach of the the two tracks (DOCA). These quantities are shown in Figure 5.3 (b) and (c) for the background. A loose pre-selection is applied to events that can not form a signal candidate ($\sim$ 50 m for IP and $\sim$ 10 m for DOCA) and they are not use to train the selection. These discriminating variables are shown separately for neutrino scattering in the air of the decay volume in Figure 5.5. The distributions vary after applying veto criteria, as shown in by the red curve in Fig. 5.5. The distribution of IP and DOCA for signal candidate is significantly narrower and shown in Fig. 5.6.
To calculate the expected background the energy range was divided into three regions: between 2 and 4 GeV, between 4 and 10 GeV and > 10 GeV. This is also done to calculate

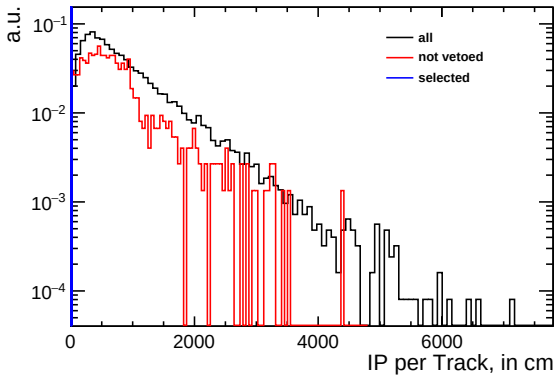

(a) IP distribution for neutrinos interacting in air

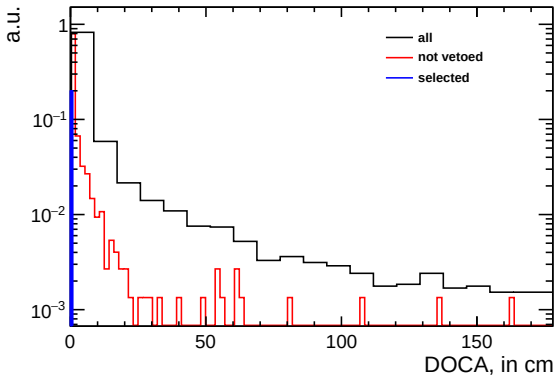

(b) DOCA distribution for neutrinos interacting in air

Figure 5.5: IP and DOCA distribution for neutrinos interacting in the air inside the non evacuated decay volume

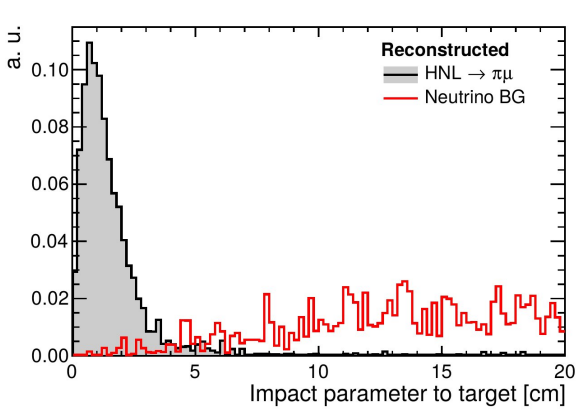

(a) IP distribution for HNLs and neutrinos interacting in the vicinity of the decay volume, close up on IP < 20 cm

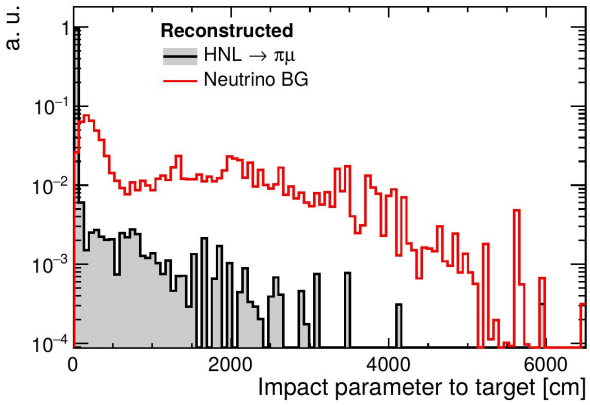

(b) IP distribution for HNLs and neutrinos interacting in the vicinity of the decay volume

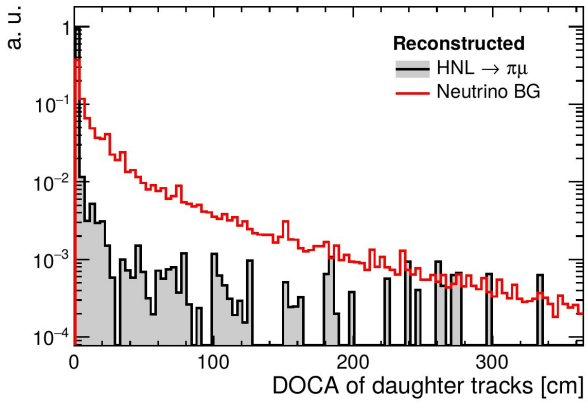

(c) DOCA distribution for HNLs and neutrinos interacting in the vicinity of the decay volume

Figure 5.6: IP and DOCA distribution for HNLs and neutrinos interacting in the vicinity of the decay volume [14]

Background source	ν (%)	$\bar{\nu}$ (%)
(p > 10.0 GeV)	0.4761	0.3205
(4.0 GeV < p < 10.0 GeV)	0.0276	0.0125
(2.0 GeV < p < 4.0 GeV)	0.0042	0.0018
total	0.5079	0.3348

Table 5.4: Reconstruction efficiency for the different energy ranges

the reconstruction efficiencies, shown in Table 5.4. The reconstruction effciency is calculated by dividing the number of reconstructed events (not weighted) by the number of total generated events. It shows that the reconstruction works best for higher energies since the particles in these events are more likely to be detected.
The expected number of neutrinos and anti-neutrinos interacting in the different detector elements are summarized in Table 5.5 and 5.6 respectively. The requirements of the columns "not vetoed" and "selected" are discussed in section 5.4. For the column "selected" no veto systems were applied. The largest source of neutrino interaction is the ν_τ-detector which is on the beam axis, however these events are easy to veto given the large number of detectors present. The second big contribution to neutrino interactions comes from the vessel walls, which are aligned with the beam axis. While they are of axis, they consists of a big amount of material and see a still relatively high neutrio flux. This allows the neutrinos to travel longer paths inside this volume which increases the probability of an interaction. The events which interact with "others" in Table 5.5 and 5.6 are mostly interacting in the UVT. The events not interacting in the UVT are interacting in the magnet of the spectrometer ($\sim$ 0.06 ($\sim$ 0.03) neutrino (anti-neutrino) events in five years of data taking).

detector	total reconstructed (%)	not vetoed (%)	selected (%)
ν detector	19480.8 (55.6)	3.2 (2.9)	0.10 (65.1)
vessel lids	315.6 (0.9)	0.9 (0.8)	0.027 (17.5)
vessel walls	14826.0 (42.3)	42.9 (38.4)	0 (0.0)
straw veto	0.2 (0.0)	0 (0.0)	0.(0.0)
tracking system	419.7 (1.2)	64.8 (57.9)	0.027 (17.5)
cave	0.4 (0.0)	0 (0.0)	0 (0.0)
others	6.3 (0.0)	0 (0.0)	0 (0.0)
total	35049.1	111.8	0.15

Table 5.5: Yields of neutrino interactions in the various elements of the facility for five years of data taking

detector	total reconstructed (%)	not vetoed (%)	selected (%)
ν detector	7113.7 (63.4)	1.4 (2.3)	0.027(66.7)
vessel lids	109.5 (1.0)	0.3 (0.5)	0 (0.0)
vessel walls	3861.0 (34.4)	31.1 (51.9)	0 (0.0)
straw veto	0.2 (0.0)	0 (0.0)	0 (0.0)
tracking system	138.1 (1.2)	27.2 (45.4)	0.014 (33.3)
cave	0.2 (0.0)	0 (0.0)	0 (0.0)
others	2.6 (0.0)	0 (0.0)	0 (0.0)
total	11225.2	60.0	0.041

Table 5.6: Yields of anti-neutrino interactions in the various elements of the facility for five years of data taking

5.4 Selection

In this section the selection criteria are discussed. The different veto systems were discussed in section 3.4. In addition a pre-selection cut (IP $<$ 10 m) was applied to further reduce the background. The rejection power of each veto systems is shown in Table 5.7 for neutrinos and in Table 5.8 for anti-neutrinos.

Veto Systems	Entries	Events / 5 years	Rejection power
Event reconstructed	890709	35049	-
SVT	149933	14809	57.7 %
UVT	159712	15395	56.1 %
SBT	38668	1347	96.2 %
IP $<$ 10m	697688	20055	42.8 %
all veto systems	3009	112	99.7 %

Table 5.7: The rejection power of the different veto systems for neutrinos interacting in the vicinity of the decay volume, each system applied separately

Veto Systems	Entries	Events / 5 years	Rejection power
Event reconstructed	599405	11225	-
SVT	76439	3877	65.5 %
UVT	83295	4061	63.8 %
SBT	50116	825	92.6 %
IP $<$ 10m	501969	7472	33.4 %
all veto systems	2650	60	99.5 %

Table 5.8: The rejection power of the different veto systems for anti-neutrinos interacting in the vicinity of the decay volume, each system applied separately

The rejection power is defined as the fraction of the events rejected by that specific veto over the total number events. In Table 5.9 and 5.10 the veto systems are applied

Applied veto system	Entries in sample	Events / 5 years	Veto efficiency
Event reconstructed	890709	35049	-
SVT	149933	14809	57.7 %
UVT	149467	14792	0.1 %
SBT	9275	534	96.4 %
IP $<$ 10m	3009	112	79.1 %

Table 5.9: The veto efficiency is the percentage of the removed events, by applying one veto after the other, for neutrinos interacting in the material surrounding the decay volume

Applied veto system	Entries in sample	Events / 5 years	Veto efficiency
Event reconstructed	599405	11225	-
SVT	76439	3877	65.5 %
UVT	76137	3872	0.2 %
SBT	6813	213	94.5 %
IP $<$ 10m	2650	60	71.8 %

Table 5.10: The veto efficiency is the percentage of the removed events, by applying one veto after the other, for anti-neutrinos interacting in the material surrounding the decay volume

subsequently to study the correlation between the different vetos. It is evident that the SVT and UVT vetos are completely correlated for neutrinos interacting in the vicinity of the decay volume. However, a certain redundancy of the veto systems will be necessary. Further studies are necessary, to conclude if both systems are necessary. In contrast the SBT shows a high rejection power and a small correlation with other veto systems. The fact, that the pre-selection cut also has a rejection power of $\sim$ 80 % shows that the veto system do not reject all physical impossible events. The SBT thus veto all events where a particle enters or leaves the decay volume.

Selection	Entries	Events / 5 years	Rejection power
Event reconstructed	7704	1959	-
SVT	7507	1909	2.6 %
UVT	7657	1947	0.6 %
SBT	685	174	91.1 %
IP $<$ 10m	5782	1470	24.9 %
all veto systems	448	114	94.2 %

Table 5.11: Rejection power for the different veto systems, applied separately to the sample of neutrinos interacting in the decay volume

The same studies were done for the decay volume filled with air and are shown in Table 5.11 - 5.14. Since the neutrinos are actually interacting inside the decay volume the SVT and UVT are not very efficient, because of their placement relative to the decay volume. The SBT is the most efficient, because it taggs all events where a particle transverse the vessel walls. The pre-selection cut is also less efficient because all the

Selection	Entries	Events / 5 years	Rejection power
Event reconstructed	8600	1133	-
SVT	8408	1107	2.2 %
UVT	8558	1127	0.5 %
SBT	906	119	89.5 %
IP $<$ 10m	6967	918	19.0 %
all veto systems	692	91	92.0 %

Table 5.12: Rejection power for the different veto systems, applied separately to the sample of anti-neutrinos interacting in the decay volume

Applied veto system	Entries	Events / 5 years	Veto efficiency
Event reconstructed	7704	1959	-
SVT	7507	1909	2.6 %
UVT	7502	1908	0.1 %
SBT	681	173	90.9 %
IP $<$ 10m	448	114	34.2 %

Table 5.13: The veto efficiency is the percentage of the removed events, by applying one veto after the other. Here the neutrinos interact with the air inside the decay volume.

interactions actually happened near the beam axis, thus only those events, which were scattered by a large angle are rejected by the pre-selection cut.
After applying the veto systems the remaining neutrino events will have to be rejected by an offline selection. The offline selection criteria were chosen to maximize the signal efficiency while removing all background. They have been optimized with the partially reconstructed signal decay HNL $\rightarrow \mu\mu\nu$, for which the di-muon system has a loose pointing to the target. Selection criteria are listed below: [14, 24]

- "1 HNL Candidate": The low cross section of producing HNLs allow to assume that no more than 1 HNL candidate will be present in one event[6].
- "Vtx in fiducial volume": To distinguish the signal from background originating from the interaction of muons and neutrinos from the material the HNl is

[6] An event can be defined as two tracks within a window of 340 ps.

Applied veto system	Entries	Events / 5 years	Veto efficiency
Event reconstructed	8600	1133	-
SVT	8408	1107	2.2 %
UVT	8402	1107	0.1 %
SBT	904	119	89.2 %
IP $<$ 10m	692	91	23.5 %

Table 5.14: The veto efficiency is the percentage of the removed events, by applying one veto after the other. Here the anti-neutrinos interact with the air inside the decay volume.

required to decay inside the fiducial volume: $|x| < 249$ cm and $|y| < 499$ cm and z starts the end of the SVT + 20 cm and ends 20 cm before the first tracking station.

- "tracks in fiducial volume": Not only the vertex has to lie in the fiducial volume also the tracks have to be inside it. Because the fiducial volume is the best controlled region, the tracks should not leave it, which is ensured by this selection.

- "N.d.f > 25": The number of degrees of freedom should be larger than 25 to have enough hits in the tracking stations.

- "DOCA < 1 cm": A large part of the background comes from two independent tracks from the same or a different interaction that after scattering in the material pass through the detector. This background can be rejected by asking a small DOCA between the two tracks. The actual value is chosen to be about 2.5 times the resolution.

- "χ^2 / N.d.f < 5": Is a quantity which represents the track quality.

- "Daughters P > 1 GeV": This selection requires that the momentum of the tracks, forming a signal candidate, have a momenta > 1 GeV.

- "IP < 0.1 m" OR "IP < 2.5m": This cut is to ensure that the particle is coming from the target and was actually produced in the experiment. The tighter cut is needed for the fully reconstructed channel HNL $\rightarrow \mu\pi$ while the looser cut is used for the partially reconstructed HNL decay channels.

- "Event not vetoed": Events remaining after having applied the veto system.

In Table 5.15 and 5.16 the selection efficiencies of the different selection criteria are shown. The selection efficiency shows how many events are selected. Also it has to be mentioned that both IP selection cuts are shown in the tables. To test the selection efficiency of the different criteria, the veto systems are applied in the end to confirm that the selection is tight enough to reject most of the neutrino background. The selection efficiencies for the HNL $\rightarrow \pi\mu$ decay channel is > 88.8 % for each selection separately [24].
The third lowest row of the tables 5.15 and 5.16 shows that the neutrino and anti-neutrino induced background can be completely rejected by the chosen selection. Even for the partially reconstructed topology the selection criteria remove almost the full background, only leaving less than one event in five years.
For neutrinos interaction in the air at atmospheric pressure inside the decay volume, the selection efficiencies are shown in Table 5.17 and 5.18. The biggest differences in the

Selection	Entries	Events / 5 years	Selection efficiency
Event reconstructed	890709	35049	-
1 HNL Candidate	679002	27635	78.8 %
Vtx in fiducial vol.	144095	5822	21.1 %
Tracks in fiducial vol.	111473	4412	75.8 %
N.d.f > 25	45131	1523	34.5 %
DOCA $<$ 1cm	7017	295	19.3 %
χ^2 / N.d.f < 5	7007	294	99.8 %
Daughters $P > 1$ GeV	5562.0	213	72.5 %
IP $<$ 0.1m	6	0.2	0.1 %
Event not vetoed	0	0.0	0.0 %
IP $<$ 2.5m	2875	76.1	35.7 %
Event not vetoed	23	0.6	0.8 %

Table 5.15: Selection efficiencies of the different criteria for neutrinos, in the evacuated experimental set up

Selection	Entries	Events / 5 years	Selection efficiency
Event reconstructed	599405	11225	-
1 HNL Candidate	471298	9019	80.3 %
Vtx in fiducial vol.	91586	1849	20.5 %
Tracks in fiducial vol.	70642	1403	75.9 %
N.d.f > 25	26481	460	32.8 %
DOCA $<$ 1cm	4252	94	20.3 %
χ^2 / N.d.f < 5	4251	93	99.9 %
Daughters $P > 1$ GeV	3328.0	66	71.0 %
IP $<$ 0.1m	3	0.0	0.1 %
Event not vetoed	0	0.0	0.0 %
IP $<$ 2.5m	1743	23.9	35.9 %
Event not vetoed	14	0.2	0.8 %

Table 5.16: Selection efficiencies of the different criteria for anti-neutrinos, in the evacuated experimental set up

selection efficiencies is the efficiency of the "Vtx in fiducial volume", "DOCA $<$ 1 cm" and "N.d.f $>$ 25". Naively it could be expected that the "Vtx in fiducial volume" should have an efficiency of 100% because the neutrinos are actually interacting inside the decay volume. But this is a cut on the reconstructed vertex and since the reconstruction is not perfect, still some events are rejected with this selection. Moreover, the efficiency of the selection "N.d.f > 25" is higher, since the particles are produced near the beam axis, and thus are more likely to traverse more tracking stations. The last significant difference in the "DOCA $<$ 1 cm" selection can also be explained by the fact that the allowed interaction region is constrained to the decay volume, thus enlarging the probability of having two tracks closer to each other.
To see where in the ν_τ-detector the neutrinos interact the plots in Figure 5.7 are shown. In Figure 5.7 (a) all interaction positions of the reconstructed events are shown. As

Selection	Entries	Events / 5 years	Selection efficiency
Event reconstructed	7704	1959	-
1 HNL Candidate	4547	1156	59.0 %
Vtx in fiducial vol.	4266	1085	93.8 %
Tracks in fiducial vol.	3421	870	80.2 %
N.d.f > 25	2488	633	72.7 %
DOCA $<$ 1cm	1357	345	54.5 %
χ^2 / N.d.f < 5	1357	345	100.0 %
Daughters $P > 1$ GeV	1240.0	315	91.4 %
IP $<$ 0.1m	5	1.3	0.4 %
Event not vetoed	3	0.8	60.0 %
IP $<$ 2.5m	283	72.0	22.8 %
Event not vetoed	35	8.9	12.4 %

Table 5.17: Selection efficiency for neutrino interaction in air of the decay volume at atmospheric pressure

Selection	Entries	Events / 5 years	Selection efficiency
Event reconstructed	8600	1133	-
1 HNL Candidate	5204	685	60.5 %
Vtx in fiducial vol.	4947	652	95.1 %
Tracks in fiducial vol.	4075	537	82.4 %
N.d.f > 25	2995	394	73.5 %
DOCA $<$ 1cm	1678	221	56.0 %
χ^2 / N.d.f < 5	1677	221	99.9 %
Daughters $P > 1$ GeV	1551.0	204	92.5 %
IP $<$ 0.1m	11	1.4	0.7 %
Event not vetoed	9	1.2	81.8 %
IP $<$ 2.5m	462	60.8	29.8 %
Event not vetoed	105	13.8	22.7 %

Table 5.18: Selection efficiency for anti-neutrino interaction in air of the decay volume at atmospheric pressure

expected, most of the interaction happen in the center but the overall shape of the interactions is elliptical and not rectangular as the actual shape of the detector. This means that in the reconstruction already events are selected, which interact in the elliptical extension of the decay volume. Figure 5.7 (b) shows the not vetoed events of the interactions in the ν_τ-detector and a similar patter is seen. To further reduce the surviving events, the ν_τ-detector could be used as a veto system, but since the performance is not known, it is not considered in this thesis and further studies are required.

Figure 5.7 (c) shows the particle produced by the interaction in the ν_τ-detector which can not be rejected by the selection criteria. The most frequent particle is the pion, which can be vetoed by the UVT. The most dangerous particle is the K_L since it can escape detection and decay in the decay volume. This mimics the signal signature, if

the co-products have no charge. The K_S and Λ_0 have short lifetimes and thus would likely decay in front of the UVT, which would then detect the decay products and veto this event.

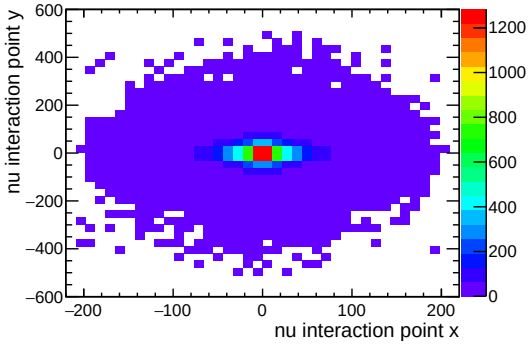

(a) Interaction position for neutrinos interacting in the ν_τ-detector

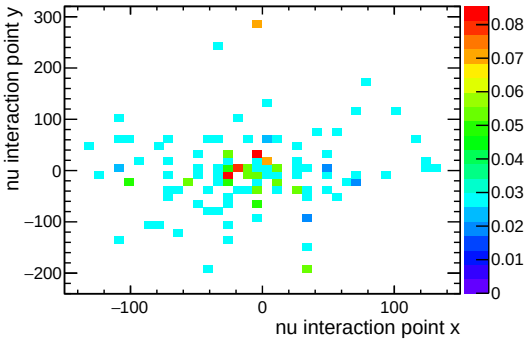

(b) Same as (a) but only for not vetoed events

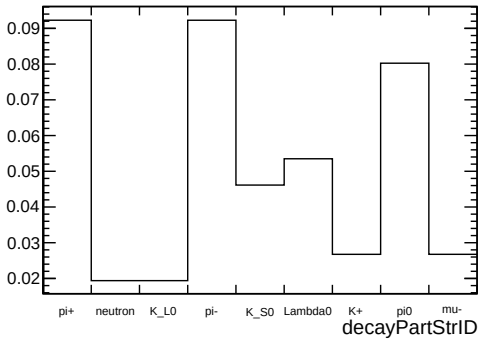

(c) Particles produced in the ν_τ-detector which are selected

Figure 5.7: Different studies of neutrinos interacting in the ν_τ-detector

Background coming from the interaction of neutrinos in the vessel walls are particularly dangerous since they can only be vetoed by the SBT. Table 5.19 and 5.20 shows in which parts of the vessel walls the interaction happened. More than > 80 % of the interactions in the vessel are in the inner wall. The veto systems are good at rejecting these events and reduce the number of events by several orders of magnitude. Also many events, which interact in the scintillator or the ribs of the vessel walls (classified as "in between the walls" in Table 5.19) can be vetoed, which is expected since they have to pass through the liquid scintillator and are likely to deposit more than the energy threshold.

	reconstructed (percentage)	not vetoed (percentage)	veto efficiency
inner wall	11917.03 (80.38 %)	41.22 (96.02 %)	99.65 %
outer wall	32.54 (0.22 %)	0 (0.0 %)	100.00 %
in between the walls	2876.42 (19.40 %)	1.71 (3.98 %)	99.94 %
walls	14826.00 (100 %)	42.92 (100 %)	99.71 %

Table 5.19: More detailed classification of the neutrino interactions in the "vessel walls" from Table 5.5. As "inner wall" is called the 3 cm thick stainless steel wall, which surrounds the decay volume. The "outer wall" is the 8 mm thick aluminum wall, which holds the liquid scintillator. Everything in between these walls (liquid scintillator itself and the ribs supporting the outer wall) is classified as "in between the walls".

	reconstructed (percentage)	not vetoed (percentage)	veto efficiency
inner wall	3171.13 (82.13 %)	30.16 (96.89 %)	99.05 %
outer wall	8.84 (0.23 %)	0 (0.0 %)	100.00 %
in between the walls	681.00 (17.64 %)	0.97 (3.11 %)	99.86 %
walls	3860.96 (100 %)	31.13 (100 %)	99.19 %

Table 5.20: More detailed classification of the anti-neutrino interactions in the "vessel walls" from Table 5.5. As "inner wall" is called the 3 cm thick stainless steel wall, which surrounds the decay volume. The "outer wall" is the 8 mm thick aluminum wall, which holds the liquid scintillator. Everything in between these walls (liquid scintillator itself and the ribs supporting the outer wall) is classified as "in between the walls".

In Figure 5.8 the direction (moving to or from the decay volume) of the particle produced by the primary neutrino interacting in the vessel wall is shown. Figure 5.8 (a) and (b) show the number of charged and neutral particles per event. Both (charged and neutral) particles are more likely to move out of the HS spectrometer. If particles are moving to the decay volume, there are no more than two particles per event moving in the same direction. Figure 5.8 (c) and (d) show the same plot as (a) and (b) but for events not rejected by the veto systems and interacting only in the inner wall, which is a 3 cm thick stainless steel wall. Particles moving to the decay volume are particularly dangerous since there are no veto systems to detect these events. Figure (c) shows that some of the charged particles are moving into the decay volume, but HNLs have no charge so these events will not be reconstructed as a HNL candidate. In Figure 5.8 (d) the neutral particles not vetoed and interaction in the inner wall are shown and very few particles are moving to the decay volume and from Table 5.5 they can be rejected by the selection. Figure 5.8 (e) and (f) show the same as (c) and (d) but for particles interacting in the outer wall and surprisingly some charged particles moving to the decay volume are not vetoed. This can be accounted to the non-perfect efficiency of the SBT. There are only very few neutral particles moving to the decay volume, which

reduces the amount of events potentially dangerous background events.

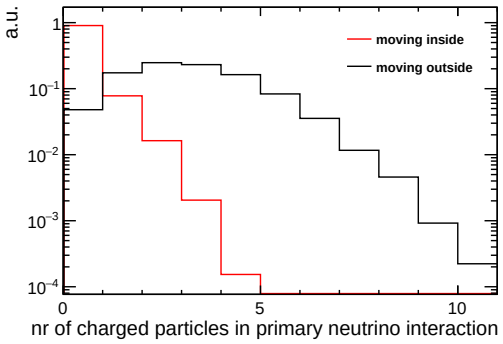

(a) Number of charged particles moving to or from the decay volume, interacting in the vessel walls

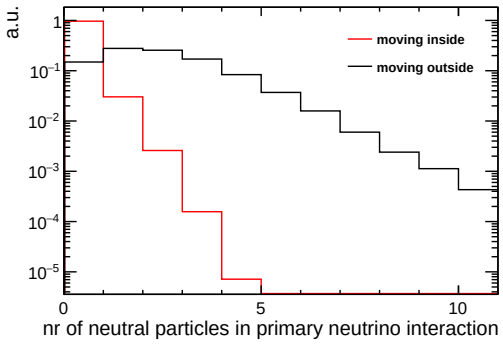

(b) Number of neutral particles moving to or from the decay volume, interacting in the vessel walls

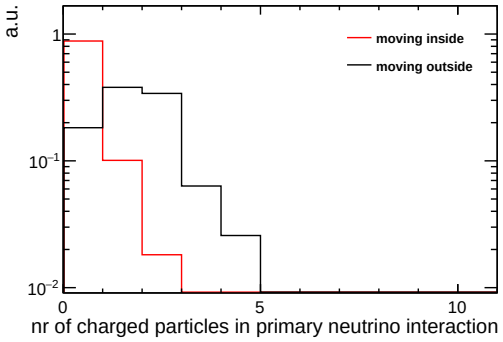

(c) Number of charged particles moving to or from the decay volume, interacting in the inner vessel walls

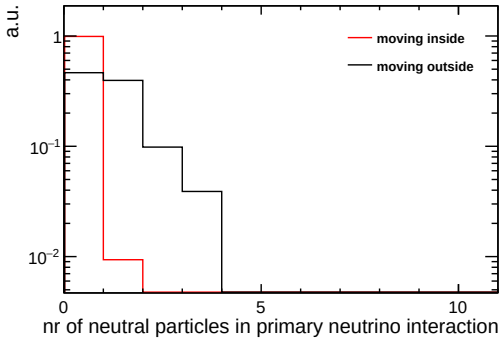

(d) Number of neutral particles moving to or from the decay volume, interacting in the inner vessel walls

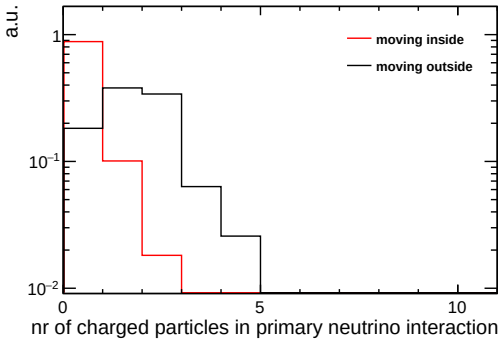

(e) Number of charged particles moving to or from the decay volume, interacting in the outer vessel walls

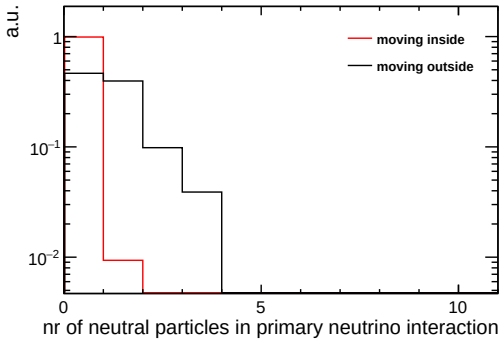

(f) Number of neutral particles moving to or from the decay volume, interacting in the outer vessel walls

Figure 5.8: Direction of daughter particles produced by the neutrino interacting in the vessel wall

6 Results

In this chapter the methods to calculate the statistical factor and the expected background, in five years of data taking, are discussed. Also a comparison between the evacuated and non evacuated experimental set up is shown.

6.1 Interactions in the surroundings

To estimate the expected background events in five years of data taking, the sample was divided into different energy ranges: 2.0 GeV/c $<$ p(ν) $<$ 4.0 GeV/c, 4.0 GeV/c $<$ p(ν) $<$ 10.0 GeV/c and p(ν) $>$ 10.0 GeV/c. In the lowest energy region the neutrino and anti-neutrino cross section (shown in Figure 6.1) is dominated by the resonant production and has some contributions of the quasi-elastic scattering. While in the second energy region (4 GeV/c $<$ p(ν) $<$ 10 GeV/c) the cross section is a mixture of the DIS and resonant production. In the last energy range the cross section is completely dominated by the DIS.

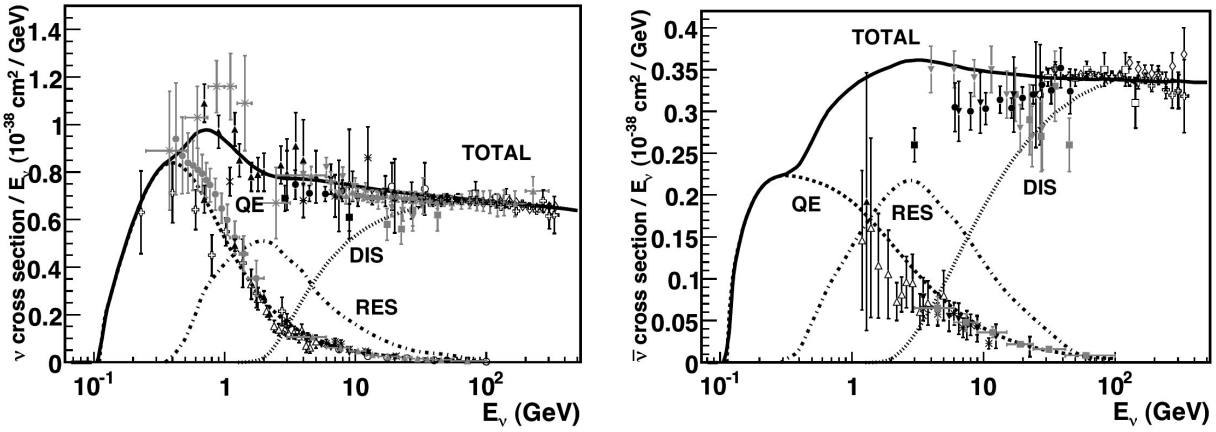

(a) Neutrino CC cross section

(b) Anti neutrino CC cross section

Figure 6.1: Total ν and $\bar{\nu}$ per nucleon charged current (CC) cross section divided by neutrino energy and plotted as a function of energy [30]. The contribution to the total cross section are also shown: quasi-elastic scattering (QE), resonant production (RES) and deep inelastic scattering (DIS)

The statistical factor is the ratio between the statistics generated and expected number of events in five years of data taking. The expected background yield for the full lifetime of the experiment if smaller than 1 event, as shown in Table 6.1 and 6.2, where the 90 % CL upper limit is reported. For the neutrino-induced background in the evacuated experimental set up, all events are rejected by the offline selection and the veto systems (see third lowest row in Table 5.15 and 5.16).

Background source	Statistical Factor	Expected Background
ν (p $>$ 10.0 GeV/c)	27.83	0.08
ν (4.0 GeV/c $<$ p $<$ 10.0 GeV/c)	11.17	0.21
ν (2.0 GeV/c $<$ p $<$ 4.0 GeV/c)	10.34	0.22
$\bar{\nu}$ (p $>$ 10.0 GeV/c)	57.05	0.04
$\bar{\nu}$ (4.0 GeV/c $<$ p $<$ 10.0 GeV/c)	22.02	0.10
$\bar{\nu}$ (2.0 GeV/c $<$ p $<$ 4.0 GeV/c)	20.90	0.11

Table 6.1: Statistical factor and expected background for the neutrino-induced background in the evacuated experimental set up. Note that the mean of a poisson distribution for which there is a 10% probability to have 0 or less events is 2.3. Therefore, the expected background is calculated by dividing 2.3 with the statistical factor.

Most of the background is expected to come from the energy range p(ν) $>$ 10.0 GeV/c, therefore a high statistics sample corresponding to about thirty times as much interaction as expected in five years of data taking has been generated. However, for all energies a sample at least the expected number of interactions was generated. The expected background level in five years of data taking is below the desired value of 0.1 events for the highest energy range, both for neutrino and anti-neutrino interactions. Also the lower energy ranges have expected background events of 0.2 events (for anti-neutrinos 0.1 events), which is near the desired limit. From the rejection power in the full energy range the background of the neutrino-induced background is well under control and at a negligible level.

6.2 Interactions in the air inside the decay vessel

In contrast to the neutrino interactions in the surroundings, for the neutrino interactions in air not all events can be rejected by the selection and veto systems (see third lowest row in Table 5.17 and 5.18). The upper limit at 90 % CL is computed by using the Poisson distribution for the observed background in the sample and divided by the statistical factor, as shown in Table 6.2.

Background source	Statistical Factor	Expected Background
ν ($p > 10.0$ GeV/c)	3.93	0.59
ν (4.0 GeV/c $< p <$ 10.0 GeV/c)	3.93	0.59
ν (2.0 GeV/c $< p <$ 4.0 GeV/c)	3.93	0.59
$\bar{\nu}$ ($p > 10.0$ GeV/c)	7.59	0.51
$\bar{\nu}$ (4.0 GeV/c $< p <$ 10.0 GeV/c)	7.59	0.51
$\bar{\nu}$ (2.0 GeV/c $< p <$ 4.0 GeV/c)	7.59	0.51

Table 6.2: Statistical factor and expected background for the neutrinos interacting in the air of the decay volume

Here the energy ranges have the same statistical power and the number of expected events is lower than the unit, but significantly larger than the desired 0.1 events in five years of data taking. This suggests the possibility to reduce drastically the costs of the decay volume. A negligible background level in five years of data taking can be achieved by using other gases inside the decay volume, instead of forcing a vacuum at 10^{-6} bar pressure. The number of reconstructed events scales with the fraction of the gas density compared to the air density. In example Helium could be used, which has a density of 0.1785 kg/m^3 which is about a factor 7 smaller than the density of air 1.293 kg/m^3. Also the statistic of the sample could be improved by simulating more events and thus increasing the stat. fact. to $>> 1$, which allow more precise estimate of the expected background.

7 Conclusion

The SHiP experiment aims to search for long living very weakly interacting particles, in particular HNLs in the GeV region, as those predicted by the νMSM. Its design consists of a heavy target, an active muon shield and a spectrometer. The HS spectrometer has a large decay volume, which is evacuated to 10^{-6} bar to minimize the neutrino interaction to have less than 0.1 events in five years of data taking. The first goal of this thesis was to study the neutrino background due to inelastic interactions in the vicinity of the decay volume, which is expected to be the main background source. A large sample of neutrino interactions, $\mathcal{O}(10^8)$, was produced to simulate the neutrino interactions in the vicinity of the decay volume. This studies showed that the expected background is less than 0.2 events for neutrino background and 0.1 events for anti-neutrino background for five years of data taking, corresponding to $2 \cdot 10^{20}$ P.o.T. Which is near the desired limit of 0.1 events to control the background to a negligible limit. The estimated cost of the HS spectrometer is 46.8 MCHF from which 11.7 MCHF (1 CHF = 0.93 EUR = 1 USD) [14] are contributed to the construction of the HS vessel. The vacuum sets demanding requirements to the construction of the vessel, which results in high costs.

The choice of the vacuum pressure is very conservative, thus as a second goal of this thesis the the case of no vacuum inside the decay volume was studied. For this reason a dedicated sample of neutrino interactions in air, interacting only inside the decay volume, was produced and analyzed. The selection and veto criteria leave a residual background corresponding to ~ 0.6 (~ 0.5) expected events for the neutrino (anti-neutrino) sample in five years of data taking.

These results do not include any cascade production from charm and beauty decays, which were implemented in FairSHiP at the end of 2015 and could not be considered for this thesis, however the results are expected to be modified at most by a factor of two. These results open up the possibility for a significant cost reduction and re-optimization of the experiment. One possibility is to fill the decay volume with a low density gas at atmospheric pressure, e.g. H_2. In addition also the muon induced background inside the decay volume (with atmospheric pressure) should be studied, to ensure that also this background can be rejected by the veto systems and the offline selection. Further studies, that start from these results, will be conducted for the re-optimization phase of the experiment.

References

[1] Laurent Canetti et al. "Dark matter, baryogenesis and neutrino oscillations from right-handed neutrinos". In: *Phys. Rev. D* 87 (9 May 2013), p. 093006. DOI: 10.1103/PhysRevD.87.093006. URL: http://link.aps.org/doi/10.1103/PhysRevD.87.093006.

[2] The ATLAS Collaboration. "Observation of a new particle in the search for the Standard Model Higgs boson with the ATLAS detector at the LHC". In: *Phys. Letter* B716 (2012) (Aug. 2012), pp. 1–29. DOI: 10.1016/j.physletb.2012.08.020.

[3] Serguei Chatrchyan et al. "Observation of a new boson at a mass of 125 GeV with the CMS experiment at the LHC". In: *Phys. Lett.* B716 (2012), pp. 30–61. DOI: 10.1016/j.physletb.2012.08.021. arXiv: 1207.7235 [hep-ex].

[4] Bogdan Povh Klaus Rith Christoph Scholz Frank Zetsche Werner Rodejohann. *Teilchen und Kerne, Eine Einführung in die physikalischen Konzepte*. 9th ed. Springer-Lehrbuch. Springer Spektrum, 2014. DOI: 10.1007/978-3-642-37822-5.

[5] The SHiP Collaboration. *A facility to Search for Hidden Particles at the CERN SPS: the SHiP physics case*. Apr. 2015. URL: http://arxiv.org/abs/1504.04855.

[6] Stefano Di Chiara, Luca Marzola, and Martti Raidal. "First interpretation of the 750 GeV di-photon resonance at the LHC". In: (2015). arXiv: 1512.04939 [hep-ph].

[7] T. Asaka, S. Blanchet, and M. Shaposhnikov. "The nuMSM, dark matter and neutrino masses". In: *Physics Letters* B.631 (Nov. 2005), pp. 151–156. DOI: 10.1016/j.physletb.2005.09.070.

[8] *SHiP - Search for Hidden Particles*. URL: http://ship.web.cern.ch/ship/.

[9] L. B. Okun. "LIMITS OF ELECTRODYNAMICS: PARAPHOTONS?" In: *Sov. Phys. JETP* 56 (1982). [Zh. Eksp. Teor. Fiz.83,892(1982)], p. 502.

[10] P. Minkowski. "mu $\rightarrow$ e gamma at a Rate of One Out of 1-Billion Muon Decays?" In: *Phys. Letter* B67 (1977), p. 421.

[11] P. A. R. Ade et al. "Planck 2013 results. XVI. Cosmological parameters". In: *Astron. Astrophys.* 571 (2014), A16. DOI: 10.1051/0004-6361/201321591. arXiv: 1303.5076 [astro-ph.CO].

[12] Hitoshi Murayama. "Theory of neutrino masses and mixings". In: *Int. J. Mod. Phys.* A17 (2002). [,495(2002)], pp. 3403–3420. DOI: 10.1142/S0217751X02012818. arXiv: hep-ph/0201022 [hep-ph].

[13] A. Gando et al. "Limit on Neutrinoless $\beta\beta$ Decay of ^{136}Xe from the First Phase of KamLAND-Zen and Comparison with the Positive Claim in ^{76}Ge". In: *Phys. Rev. Lett.* 110 (6 Feb. 2013), p. 062502. DOI: 10.1103/PhysRevLett.110.062502. URL: http://link.aps.org/doi/10.1103/PhysRevLett.110.062502.

[14] The SHiP Collaboration. *A facility to Search for Hidden Particles (SHiP) at the CERN SPS*. Technical Proposal. SHiP Collaboration, Apr. 2015. URL: http://arxiv.org/abs/1504.04956.

[15] Johannes Blümlein and Jürgen Brunner. "New Exclusion Limits on Dark Gauge Forces from Proton Bremsstrahlung in Beam-Dump Data". In: *Phys. Lett.* B731 (2014), pp. 320–326. DOI: 10.1016/j.physletb.2014.02.029. arXiv: 1311.3870 [hep-ph].

[16] Edda Gschwendtner et al. "Performance and Operational Experience of the CNGS Facility". In: *Conf. Proc.* C100523 (2010), THPEC046.

[17] F. Hahn et al. *NA62 Technical Design Document*. Tech. rep. NA62-10-07. NA62 at CERN, Dec. 2010. URL: https://na62.web.cern.ch/na62/Documents/TechnicalDesign.html.

[18] Rene Brun and Fons Rademakers. "ROOT — An object oriented data analysis framework". In: *Nuclear Instruments and Methods in Physics Research Section A: Accelerators, Spectrometers, Detectors and Associated Equipment* 389.1–2 (1997). New Computing Techniques in Physics Research V, pp. 81–86. ISSN: 0168-9002. DOI: http://dx.doi.org/10.1016/S0168-9002(97)00048-X. URL: http://www.sciencedirect.com/science/article/pii/S016890029700048X.

[19] The GENIE Collaboration. *The GENIE Neutrino Monte Carlo Generator PHYSICS & USER MANUAL*. June 2013.

[20] Torbjorn Sjostrand, Stephen Mrenna, and Peter Z. Skands. "A Brief Introduction to PYTHIA 8.1". In: *Comput. Phys. Commun.* 178 (2008), pp. 852–867. DOI: 10.1016/j.cpc.2008.01.036.

[21] Torbjorn Sjostrand, Stephen Mrenna, and Peter Z. Skands. "PYTHIA 6.4 Physics and Manual". In: *JHEP* 05 (2006), p. 026. DOI: 10.1088/1126-6708/2006/05/026.

[22] The GEANT Collaboration. *GEANT4*. Oct. 2015. URL: https://geant4.web.cern.ch/geant4/.

[23] J. Kempa and A. Krawczynska. "Low energy muons in the cosmic radiation". In: *Nucl. Phys. Proc. Suppl.* 151 (2006). [,299(2006)], pp. 299–302. DOI: 10.1016/j.nuclphysbps.2005.07.056.

[24] SHiP Collaboration. *Addendum to Technical Proposal: A Facility to Search for Hidden Particles (SHiP) at the CERN SPS*. Tech. rep. CERN-SPSC-2015-040. SPSC-P-350-ADD-2. Geneva: CERN, Oct. 2015. URL: https://cds.cern.ch/record/2060742.

[25] Dmitry Gorbunov and Mikhail Shaposhnikov. "How to find neutral leptons of the νMSM?" In: *JHEP* 10 (2007). [Erratum: JHEP11,101(2013)], p. 015. DOI: 10.1007/JHEP11(2013)101,10.1088/1126-6708/2007/10/015. arXiv: 0705.1729 [hep-ph].

[26] Laurent Canetti and Mikhail Shaposhnikov. "Baryon Asymmetry of the Universe in the NuMSM". In: *JCAP* 1009 (2010), p. 001. DOI: 10.1088/1475-7516/2010/09/001. arXiv: 1006.0133 [hep-ph].

[27] Dmitry Gorbunov and Mikhail Shaposhnikov. "How to find neutral leptons of the νMSM?" In: *Journal of High Energy Physics* 2007.10 (2007), p. 015. URL: http://stacks.iop.org/1126-6708/2007/i=10/a=015.

[28] D. Gorbunov, A. Makarov, and I. Timiryasov. "Decaying light particles in the SHiP experiment: Signal rate estimates for hidden photons". In: *Phys. Rev.* D91.3 (2015), p. 035027. DOI: 10.1103/PhysRevD.91.035027. arXiv: 1411.4007 [hep-ph].

[29] Rouven Essig et al. "Working Group Report: New Light Weakly Coupled Particles". In: *Community Summer Study 2013: Snowmass on the Mississippi (CSS2013) Minneapolis, MN, USA, July 29-August 6, 2013*. 2013. arXiv: 1311.0029 [hep-ph]. URL: http://inspirehep.net/record/1263039/files/arXiv:1311.0029.pdf.

[30] J. A. Formaggio and G. P. Zeller. "From eV to EeV: Neutrino Cross Sections Across Energy Scales". In: *Rev. Mod. Phys.* 84 (2012), p. 1307. DOI: 10.1103/RevModPhys.84.1307. arXiv: 1305.7513 [hep-ex].